Swiss J Geosci (2010) 103:61–82
DOI 10.1007/s00015-010-0007-3

The Moslavačka Gora crystalline massif in Croatia: a Cretaceous heat dome within remnant Ordovician granitoid crust

Biljana Starijaš · Axel Gerdes · Dražen Balen ·
Darko Tibljaš · Fritz Finger

Received: 16 March 2009 / Accepted: 27 November 2009 / Published online: 28 May 2010

Abstract For a long time the Moslavačka Gora Massif in Croatia has been regarded as a major outcrop of Variscan crystalline basement of the South Tisia block. However, new geochronological data indicate that this massif consists of a Cretaceous S-type granite pluton intruding a Cretaceous low-pressure/high-temperature (LP/HT) metamorphic envelope. The age of the LP/HT metamorphism is estimated at $\sim$90–100 Ma using the method of electron microprobe based monazite dating. The Central Granite was dated at 82 $\pm$ 1 Ma (LA-SF-ICP-MS zircon age). The metamorphic complex comprises mainly felsic anatexites and orthogneisses of granitic composition, some metapelites (paragneisses and mica schists) and amphibolites. Zircons from three different samples of metagranite were dated at 486 $\pm$ 6, 483 $\pm$ 6, and 491 $\pm$ 1 Ma, suggesting that most of the metamorphic complex represents an Early Ordovician granitic series. The Cretaceous regional metamorphism culminated in granulite facies conditions of $\sim$750°C and 3–4 kbar. A retrograde metamorphic event at lower amphibolite facies conditions overprinted the metamorphic complex. This event is probably related to the intrusion of the Central Granite. The southeastern sector of the massif was additionally affected by post-granitic, predominantly NE oriented shearing at greenschist facies conditions. As yet there is no clear evidence for Variscan events in the Moslavačka Gora Massif. Mineral relics of a medium-pressure amphibolite facies metamorphism are preserved in amphibolites. They are older than the Cretaceous LP/HT regional metamorphism, but their age is presently unknown. Some indications for a Permian regional metamorphic event are provided by inherited zircons in the Central Granite that have been dated with a Permian age, and by Permian monazite relics in metapelites. The Cretaceous high heat flow regime recorded in the Moslavačka Gora Massif is unique in the subcrop of the Pannonian Basin and may be a local feature triggered by a mafic intrusion in the lower crust.

Keywords Moslavačka Gora · Sava Zone · Ordovician granitoids · Cretaceous LP/HT metamorphism

Editorial handling: Edwin Gnos.

B. Starijaš (✉) · F. Finger
Fachbereich Materialforschung und Physik,
Universität Salzburg, Hellbrunnerstrasse 34,
5020 Salzburg, Austria
e-mail: biljana.starijas2@sbg.ac.at

A. Gerdes
Geozentrum, Facheinheit Mineralogie,
Goethe Universität, Altenhöferallee 1,
60438 Frankfurt am Main, Germany

D. Balen · D. Tibljaš
Institute of Mineralogy and Petrology, University of Zagreb,
Horvatovac 95, 10000 Zagreb, Croatia

Geological setting and previous work

The Moslavačka Gora Massif in Croatia (MGM) is located about 50 km ESE of Zagreb (Fig. 1). It covers an area of $\sim$180 km^2 and represents one of the major surface exposures of crystalline basement within the Tertiary sediments of the Pannonian Basin (Pamić 1990; Pamić et al. 2002a). The massif is interpreted as a horst structure that formed by vertical faulting in the Miocene (Korolija et al. 1986).

In terms of the Alpine plate tectonic framework, the MGM has been long considered to be part of the Tisia block (Pamić 1998; Pamić et al. 2000; Pamić and Jurković 2002), which forms the innermost parts of the northwestern Dinarides and

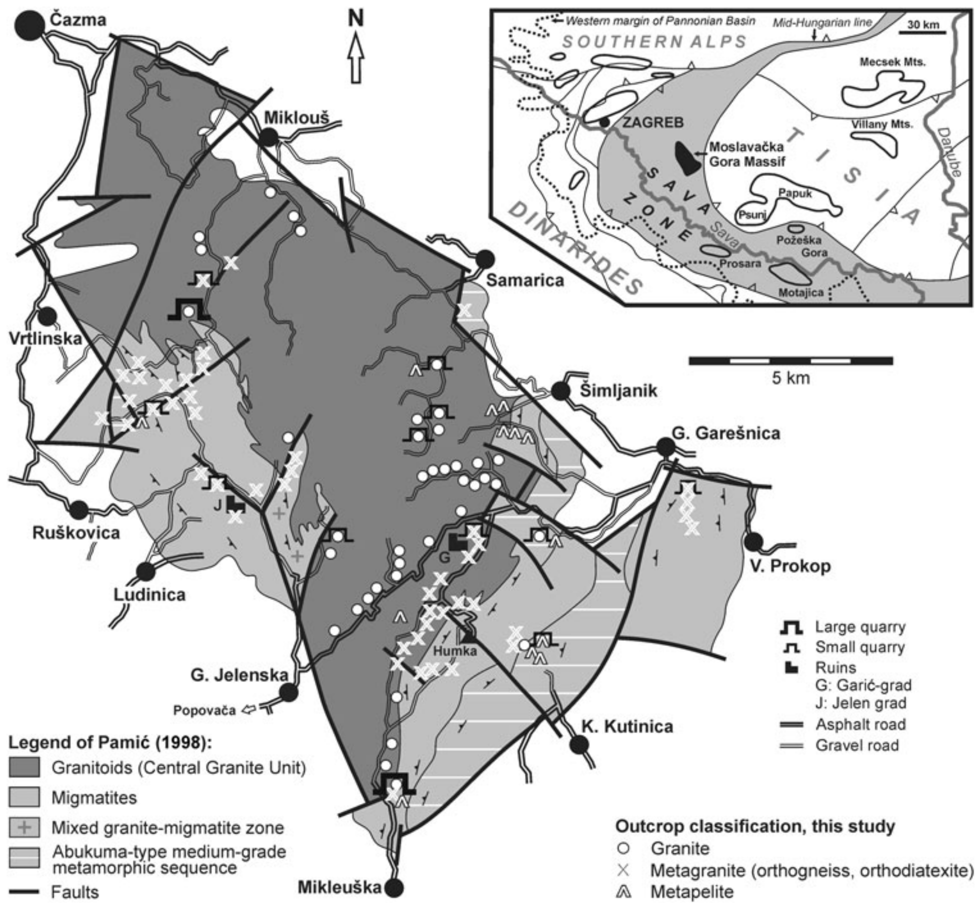

Fig. 1 Geological sketch map of the Moslavačka Gora Massif after Pamić (1998). *White symbols* are the sampling sites of the present study and indicate the predominant rock type found in the particular outcrops. *Inset* shows the major basement massifs in the Pannonian Basin and their position within the Alpine tectonic framework (based on Schmid et al. 2008)

the Romanian Carpathians (Schmid et al. 2004). The Mid-Hungarian line (Csontos and Nagymarosy 1998) separates Tisia from the northerly adjacent eastern extension of the Southern Alps and the SW-NE-striking continuation of the internal Dinarides situated NE of Zagreb (Schmid et al. 2004). Recently, Ustaszewski et al. (2008) and Schmid et al. (2008) related the MGM to the so-called "Sava Zone", which is believed to host the suture between Tisia and the Northern Dinarides (Fig. 1). Reliable information concerning the geological evolution of the massif was until now not available, so that any correlation with neighbouring basement units has remained largely speculative. This study was carried out with aim of providing modern petrographic and, in particular, geochronological data for the rocks of the MGM.

A geological overview map of the MGM is available in Pamić (1998). He distinguished between a *Central Granite Unit* (a two-mica S-type granite pluton) and metamorphic rocks at the periphery of the massif. The metamorphic rocks were divided into *Migmatites* and *Abukuma-type medium-grade metamorphic rocks* (Fig. 1), the latter comprising mainly paragneisses and mica schists. According to Pamić (1998) the migmatites evolved from the Abukuma-type medium-grade paragneiss series during a LP/HT ultrametamorphic event, which is also considered responsible for the formation of the Central Granite. It was speculated that K metasomatism played a significant role during that process (Pamić 1990).

Derived from the fact that LP/HT ultrametamorphic events are particularly typical for the Variscides (Zwart and Dornsiepen 1978; O'Brien 2000), it was the common opinion that the metamorphic rocks of the MGM represent a Variscan basement (Pamić 1998; Pamić et al. 2000; Balen et al. 2001; Pamić et al. 2002a). Cretaceous K–Ar and Ar–Ar mica ages that were recorded in various parts of the massif (Lanphere and Pamić 1992; Palinkaš et al. 2000; Balen et al. 2001) were considered as dating a metamorphic overprint during the Alpine orogeny (Lanphere and Pamić 1992; Pamić 1998; Pamić and Jurković 2002).

Small occurrences of amphibolite layers within migmatites and metapelites were studied by Pamić et al. (2002a). Relicts of a medium pressure metamorphic mineral paragenesis were recognized in these rocks. This older metamorphic paragenesis was strongly overprinted but not completely obliterated during the LP/HT event. The amphibolites thus provide the important information that the metamorphic history of the MGM was polyphase.

Petrography and geochemistry

Overview

During this study a large number of samples were collected from all parts of the massif (Fig. 1). We distinguished the following principle rock types:

Granite of the Central Granite Unit: Fine to medium grained two-mica granite, normally undeformed and unmetamorphosed.

Metagranite: High grade metamorphic (anatectic) rocks of granitic composition (orthogneisses, diatexites), derived from a granitic protolith. These metagranitic rocks are the main constituents of the Migmatite zone (Fig. 1) of Pamić (1998).

Metapelite: Paragneisses and mica schists; these rocks occur mainly in the southeastern part of the massif.

Amphibolitic rocks (Pamić et al. 2002a) form only small bodies and were not sampled.

Field work showed that the foliation of the metamorphic rocks in the western sector of the massif (mainly metagranite) is mostly oriented NW. This has been already noted by Pamić (1990). The adjacent Central Granite was not affected by this phase of deformation. However, in the southeastern sector of the MGM, a younger, preferentially NE oriented foliation can be observed, which affected also the southeastern fringe of the Central Granite Unit.

The metapelites

The metapelites comprise mainly biotite paragneisses and biotite-muscovite paragneisses often containing some cordierite, sillimanite or andalusite, but rarely garnet. Mica schists are occasionally interlayered in these paragneisses and have the same mineral compositions but with subordinate quantities of feldspars (Barić 1954; Balen and Pamić 2000). The largest occurrences of metapelites are in the southeastern part of the MGM (Fig. 1), which is strongly overprinted by NE oriented foliation. Thin-section observations suggest that this deformation occurred mainly at mid greenschist facies temperatures. This is inferred from the fact that the feldspars generally show a brittle behavior, and that the shear bands consist mainly of muscovite, some chlorite and fine grained recrystallized quartz. However, pseudomorphs replacing garnet and cordierite reveal an earlier higher grade LP/HT metamorphic history.

West of Humka mountain, metapelites are less affected by retrogression. A key sample (BS 10) contains garnet with a size ~2 mm, as well as relics of fresh cordierite. The peak paragenesis in this sample is garnet + cordierite + plagioclase + sillimanite + K-feldspar + quartz (Fig. 2). In addition, a number of retrograde mineral reactions can be identified in thin-section. The garnet is marginally replaced by biotite. The primary plagioclase (bytownite) is overgrown by an andesine rim (Pl II in Fig. 2). K-feldspar and sillimanite reacted to symplectitic muscovite–quartz intergrowths. The cordierite is replaced by muscovite and biotite. In some places, andalusite has formed together with muscovite and biotite (Fig. 2), possibly at the expense of former cordierite.

Microprobe analyses show that the garnets are zoned (Fig. 3) with a relatively homogenous core zone ($Alm_{84}Prp_7Sps_5Grs_4$) and a Mn-rich, Mg-depleted rim zone ($Alm_{80}Prp_{4-5}Sps_{8-16}Grs_4$). This kind of garnet zoning can be interpreted in terms of retrograde resorption and diffusive reequilibration of the garnet rim (Spear et al. 1999). The cordierite grains are unzoned and have a uniform composition. In contrast, many plagioclases show an internal variation from $\sim An_{70-80}$ in the core zone to $\sim An_{35-40}$ in the rim zone. Muscovite is again of widely constant composition, independent of its microstructural position, whereas biotite in cordierite pseudomorphs is slightly higher in its Mg number than the remainder of the biotite. Representative mineral compositions used for P–T calculations are listed in Table 1.

Based on the Grt–Crd Fe–Mg exchange thermometer (Thompson 1976; Holdaway and Lee 1977; Perchuk 1991) peak temperatures in the range of 720–770°C can be estimated. A pressure estimation is possible with the GASP barometer (Koziol 1989), as the critical paragenesis of this barometer (Grt–Sil–Pl–Qtz) was present at the P–T peak. Using the core compositions of plagioclase and garnet (Table 1) this barometer yields pressures of 3–4 kbar for the high-T metamorphic stage.

Regarding the retrograde path, the appearance of andalusite (Fig. 2) attests a pressure below 4 kbar (Spear et al. 1999). The Grt–Bt thermometer (using garnet rim compositions and adjacent biotites) gives temperatures in the range of ~550–630°C at 1–3 kbar, depending on the calibration chosen (Holdaway 2000; Holdaway et al. 1997; Gessmann et al. 1997; Kleeman and Reinhardt 1994). The muscovite–biotite thermometer of Hoisch (1989) gives somewhat lower temperatures of 520–540°C (at 1–3 kbar), as does the plagioclase–white mica K–Na exchange thermometer of Green and Usdansky (1986). Therefore, the main phase of recrystallization in sample BS 10 has most probably taken place at temperature conditions of the lower amphibolite facies.

The metagranites

The mineral paragenesis of these rocks is K-feldspar + plagioclase + quartz + biotite + secondary muscovite + subordinate cordierite, garnet and rarely sillimanite (Pamić 1990). Although of similar modal composition (30–40 vol% Qtz, 30–40 vol% Kfs, 20–30 vol% Pl, 3–10 vol% Bt),

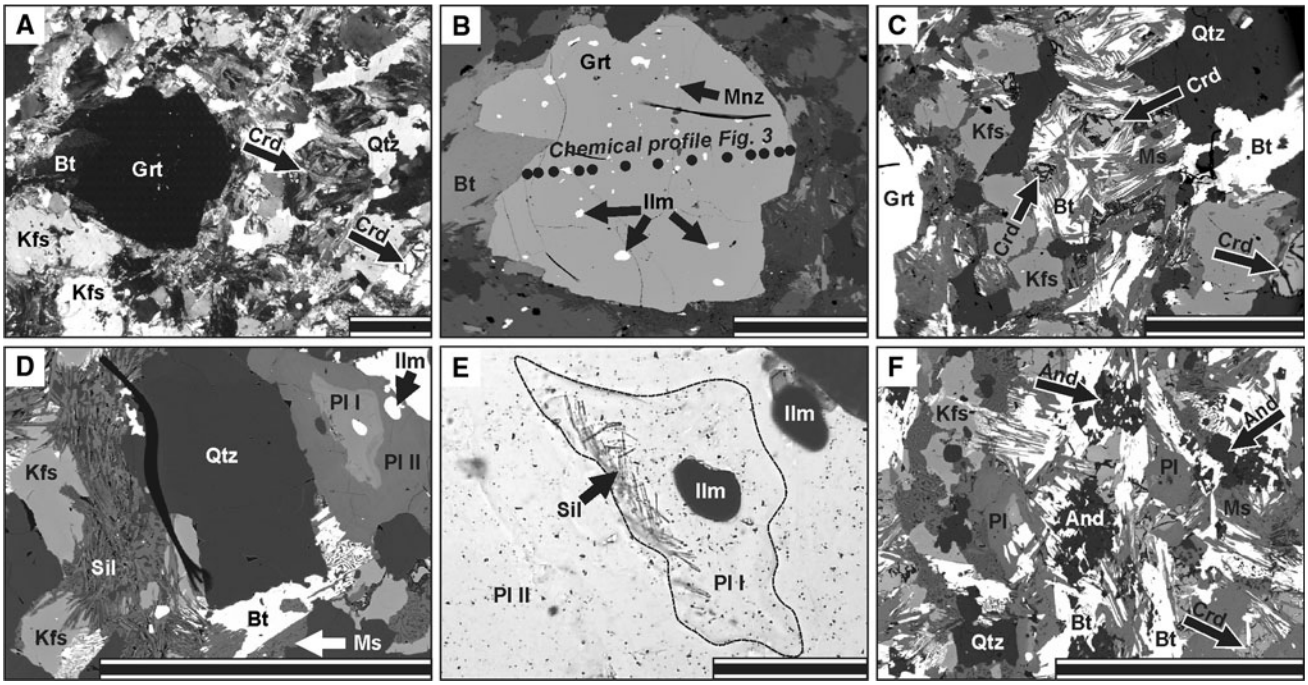

Fig. 2 Photomicrographs and backscatter electron (BSE) images illustrating minerals and microstructures in metapelite sample BS 10. *Scale bars* are 1 mm. Mineral abbreviations are according to Kretz (1983). **a** Larger grains of garnet, cordierite (partly altered), K-feldspar and quartz are relics of the original high-T paragenesis and are embedded in a fine-grained retrograde matrix consisting mainly of quartz, plagioclase and micas (photomicrograph; crossed polarizers). **b**, **c** Details from **a** (BSE images) showing the marginal replacement of garnet by biotite, and the pseudomorphic replacement of cordierite by biotite and muscovite. *Arrows* indicate fresh cordierite relics. **d** Sillimanite and An-rich plagioclase (Pl I) also belong to the peak paragenesis. Pl I ($\sim An_{75}$) is replaced and overgrown by a younger plagioclase (Pl II) with lower An content (BSE image). **e** Close-up of the zoned plagioclase from **d**, showing that the An-rich core zone (Pl I) encloses needles of sillimanite (photomicrograph; plane light). **f** Andalusite grains in quartz–mica matrix (BSE image)

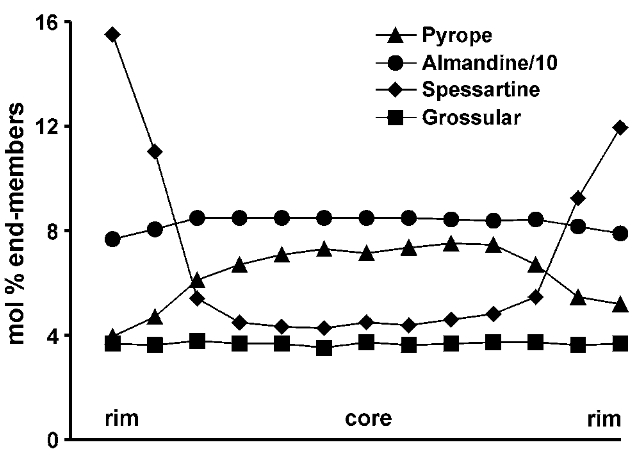

Fig. 3 Compositional profile through garnet from sample BS 10 (grain and position of analyses points are shown in Fig. 2b)

a large variability in terms of texture and grainsize is observed (Fig. 4). Metagranites with a gneissic fabric (Fig. 4a, c, f) alternate with diatexitic types (Fig. 4b, d, e) with a nebulitic texture (Mehnert 1968). Both, gneissic and diatexitic metagranites can often be found in the same outcrop with gradual transitions.

An attempt was made to divide the metagranites of the MGM into different subtypes. Metagranites that contain relics of primary K-feldspar megacrysts with a size of 1–2 cm are referred to as *Jelen grad type metagranites* throughout this paper (Fig. 4a, b). Such Kfs-phyric metagranites are widespread in the MGM. The modal composition is always granitic with roughly equal amounts of K-feldspar, plagioclase and quartz. Biotite (5–10 vol%) is the major mafic mineral, although some garnet and cordierite are commonly found in darker, biotite rich layers. Both, garnet and cordierite are always strongly resorbed and have reacted back to micas. Round biotite patches (0.5–1 cm), found in some of the diatexitic Jelen grad metagranites (e.g. in the quarry N of Mikleuška), are likely to represent former garnet. The widespread relics (pseudomorphs) of garnet and cordierite are important genetic indicators, because they document that the metagranites experienced basically the same LP/HT metamorphic conditions as the metapelites.

In the area around the Garić-grad ruin, fine grained metagranites (both gneissic and diatexitic variants) are exposed. These *Garić-grad type metagranites* (Fig. 4c, d) are obviously derived from a fine grained granite protolith.

Table 1 Representative mineral analyses from metapelite sample BS 10

	Grt core	Grt rim	Crd	Pl 1	Pl 2	Bt Grt[a]	Bt in Crd	Ms	And
SiO_2	36.24	36.40	47.67	48.84	57.87	32.58	33.86	47.61	36.10
TiO_2	0.08	0.00	0.00	0.08	0.04	3.13	2.35	0.20	0.08
Al_2O_3	20.68	20.27	32.21	32.85	27.01	20.06	20.25	37.30	62.64
FeO	37.39	34.85	13.08	0.00	0.00	25.35	23.32	1.06	0.40
MnO	1.85	6.89	0.47	0.00	0.00	0.21	0.24	0.00	0.02
MgO	1.80	0.99	4.57	0.00	0.00	4.09	5.92	0.27	0.08
CaO	1.20	1.29	0.02	15.94	7.86	0.00	0.00	0.01	0.10
Na_2O	0.00	0.00	0.11	2.34	7.14	0.13	0.12	0.29	0.01
K_2O	0.00	0.00	0.00	0.04	0.16	9.99	10.13	9.14	0.00
Total	99.23	100.68	98.13	100.08	100.07	95.55	96.20	95.88	99.43
O	12	12	18	8	8	11	11	11	5
Si	2.969	2.973	5.026	2.226	2.580	2.566	2.613	3.099	0.983
Ti	0.005	0.000	0.000	0.003	0.001	0.185	0.136	0.010	0.002
Al	2.000	1.952	4.002	1.764	1.419	1.861	1.841	2.861	2.007
Fe	2.564	2.376	1.155	0.000	0.000	1.671	1.507	0.058	0.009
Mn	0.128	0.479	0.042	0.000	0.000	0.014	0.016	0.000	0.001
Mg	0.219	0.121	0.718	0.000	0.000	0.481	0.681	0.027	0.003
Ca	0.106	0.113	0.002	0.778	0.376	0.000	0.000	0.001	0.003
Na	0.000	0.000	0.022	0.207	0.617	0.020	0.018	0.036	0.001
K	0.000	0.000	0.000	0.002	0.009	1.003	0.998	0.759	0.000

[a] Adjacent to garnet

Like in the Jelen grad metagranites, relics of garnet and cordierite can be found.

In the area SE of Vrtlinska, a distinct type of an aphyric, particularly K-feldspar rich (35–40 vol%) diatexite is often found (*Vrtlinska diatexite*, Fig. 4e). Similar rocks are also exposed east of the Jelen grad ruin. They were mapped by Pamić (1998) as "mixed granite–migmatite zone" (Fig. 1), and considered as infiltrated with magma from the Central Granite pluton. From field evidence it appears equally possible to interpret the rock as anatexite containing a high amount of in situ partial melt. In thin-section, the Vrtlinska diatexite displays an igneous fabric, with evenly distributed, subhedral feldspar and interstitial quartz. Plagioclase (~25 vol%) of isometric shape (1–3 mm) is typically unzoned. K-feldspar forms large (3–5 mm), moderately elongated, subhedral crystals with Carlsbad twinning, but can also be interstitial. Biotite (3–7 vol%) is small and mostly euhedral. Unlike the feldspars, the small biotite flakes show often an orientation and an inhomogeneous, layered distribution in the rock (Fig. 4e). Small accessory garnet can sometimes be seen. Some muscovite formed secondary at the expense of biotite.

In the quarry south of Gornja Garešnica (Fig. 1) and in its surroundings, a coarse, quartz-rich flazer gneiss is exposed (Fig. 4f). Microtextures suggest that this rock was strongly affected by greenschist facies deformation. However, due to the particularly quartz-rich composition (40 vol%), this rock is also considered as a distinct protolithic type of metagranite. Geochemically similar metagranites, but with a diatexitic texture, have been found also W of Humka. These show biotite patches interpreted as retrogressed garnet or cordierite.

In order to better characterize the metagranites of the MGM, a geochemical study was carried out. More than 20 large samples (1–2 kg) were analyzed by X-ray fluorescence methods (Table 2). Analyses were carried out on a Bruker S4 Pioneer instrument, equipped with a 4 kW Rh tube. Major elements were determined on glass beads at reduced tube energies. Counting times were chosen in a way that the relative 2σ uncertainties were better than 1% for SiO_2 and Al_2O_3, and better than 5% for elements at the 1–10 wt% concentration level. For trace elements, which were measured on pressed powder pellets, counting times and tube conditions were optimized automatically per element (up to 4 kW and 400 s), to obtain a detection limit of at least 3 ppm. Typical errors (2σ) from the counting statistics were 1–2 ppm at low concentrations (<10 ppm), 2–5 ppm at the 10–100 ppm concentration level, and better than 5% (relative) for the rest.

Data show that the metagranites are generally SiO_2 rich (68–76 wt%) and of high-K nature ($K_2O > 3.5$ wt%). The Jelen grad type metagranites are strongly peraluminous with A/CNK ratios between 1.1 and 1.3. They thus seem to represent an S-type granite suite (Chappell and White

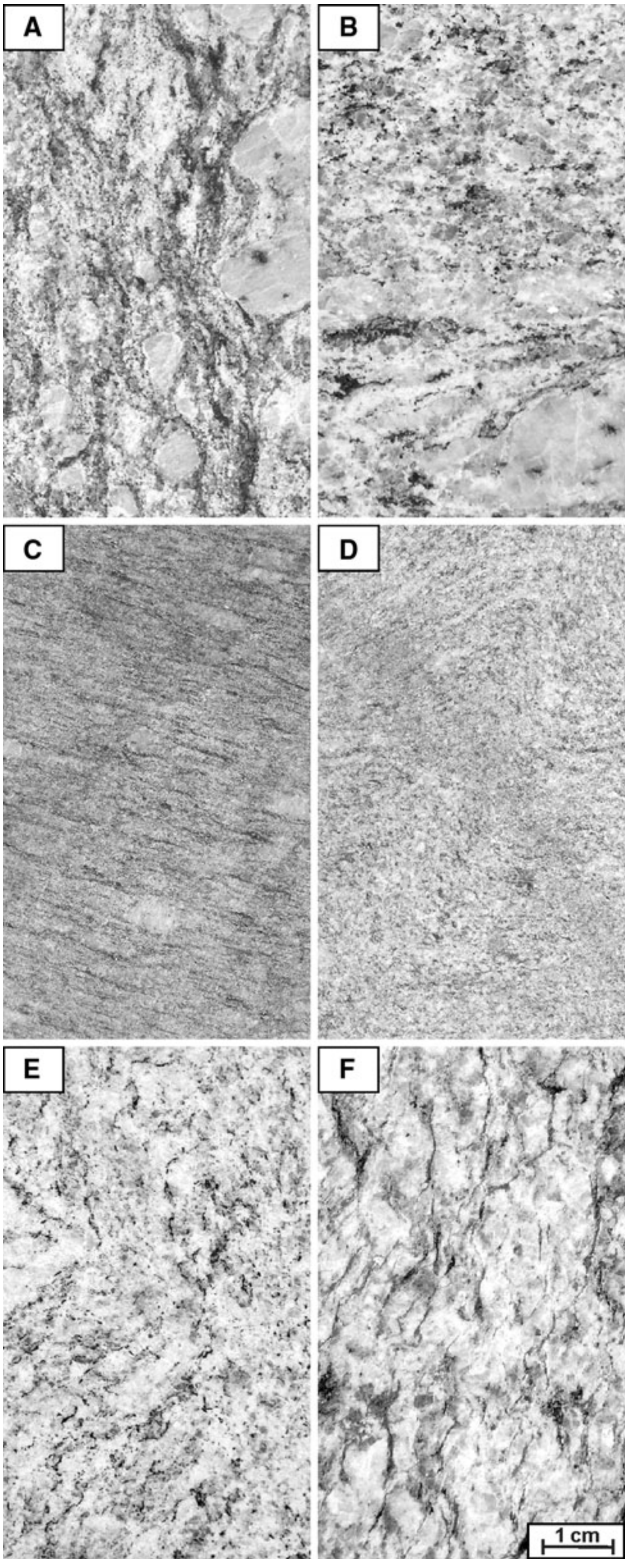

Fig. 4 Macroscopic appearance of the metagranites from the Moslavačka Gora Massif. **a**, **b** Jelen grad type metagranites from Humka (orthogneiss) and near Jelen grad ruin (diatexitic). **c**, **d** Garić-grad type metagranites from Garić-grad quarry (orthogneiss) and near Garić-grad ruin (diatexitic). **e** Vrtlinska diatexite. **f** Flazer gneiss from Gornja Garešnica. All pictures in same magnification

1974). The fine grained metagranites from Garić-grad are less peraluminous (A/CNK 1–1.05). They show particularly high Zr and Y contents (Fig. 5) and elevated Ga/Al ratios (Table 2) characteristic of A-type granites (Collins et al. 1982). Neither in the Jelen grad nor the Garić-grad group, systematic geochemical differences between gneissic and diatexitic varieties have been encountered, implying that metasomatism played no major role during high-grade metamorphism and anatexis, and that the recorded geochemical features are, in general, protolithic.

The flazer gneiss sample from south of Gornja Garešnica (Fig. 4f) and the quartz-rich diatexites from W of Humka display similar geochemical features, such as high SiO_2 (74–76 wt%) at peraluminous A/CNK ratios (1.1–1.25), high Rb (250–280 ppm), low Sr (<50 ppm) and low Ba contents (Table 2), and do not fall on the chemical trends defined by the Jelen grad and Garić-grad type granitoids (Fig. 5). These rocks thus appear to define a third magmatic suite within the metagranite complex.

Finally, the microcline rich metagranites from the western MGM (Vrtlinska diatexite) define an independent geochemical group. Although these rocks are moderately peraluminous (A/CNK 1.1–1.2), they are low in P. This can be taken as an argument that they contain no melt component from the Central Granite Unit, which represents a high-P, S-type magma. Based on diagrams like P_2O_5 versus Y (Fig. 5), the previous interpretation of the Vrtlinska diatexite as contaminated Central Granite must be considered unlikely. Chemical data are more compatible with an interpretation as an anatexite with a high proportion of partial melt.

The Central Granite Unit

The Central Granite Unit of the MGM consists mainly of fine-grained, two-mica, S-type granites. The coarsest variants contain feldspars with a length of ~7 mm, but the average grain size is 1–3 mm (Fig. 6). The granite is mostly undeformed, sometimes a slight magmatic orientation of the biotite is visible. However, in the southeastern MGM, the Central Granite was clearly affected by subsolidus deformation. This led in places to the development of mylonites (e.g. quarry N of Mikleuška, Fig. 6c). The brittle behaviour of the feldspar coupled with a strong recrystallization of quartz and biotite shows that these mylonites formed mainly under greenschist facies conditions.

The Central Granite of the MGM is mostly of granitic composition (s.s.). A few samples plot in the granodiorite field of the Streckeisen diagram. Biotite contents are typically 4–8 vol%, muscovite contents 3–7 vol%. Some biotite is early magmatic and enclosed in plagioclase. The K-feldspar is relatively late in the crystallization

Table 2 Geochemical data for rocks from the Moslavačka Gora Massif (XRF analyses, major elements in wt%, trace elements in ppm, LOI = Loss on ignition, bdl = below detection limit)

Rock sample	CG BS 37	CG BS 38	GD BS 2	JG BS 35	JG BS 36G	GG BS 3	GG BS 17	VT BS 32	VT BS 34	GT BS 54
SiO_2	71.58	72.66	74.45	71.94	73.93	73.89	73.21	74.15	75.47	75.84
TiO_2	0.32	0.29	0.16	0.39	0.37	0.30	0.31	0.19	0.20	0.13
Al_2O_3	14.63	14.64	13.33	14.69	13.63	12.99	13.17	14.23	13.75	13.26
Fe_2O_3	2.13	1.77	1.23	2.37	2.18	2.69	2.94	1.29	1.09	1.26
MnO	0.05	0.04	0.02	0.03	0.03	0.05	0.05	0.02	0.01	0.03
MgO	0.72	0.42	0.33	0.57	0.50	0.45	0.35	0.32	0.27	0.18
CaO	1.16	1.19	0.89	1.55	1.69	1.41	1.49	0.74	0.89	0.52
Na_2O	3.04	3.40	3.46	3.21	3.26	3.75	3.38	3.78	3.86	3.43
K_2O	4.49	4.62	4.49	3.98	3.53	3.90	4.11	4.63	4.37	4.77
P_2O_5	0.20	0.22	0.22	0.17	0.17	0.10	0.10	0.09	0.07	0.24
LOI	1.40	0.98	1.00	1.42	0.88	0.83	0.57	1.10	0.72	1.03
Total	99.72	100.23	99.58	100.32	100.17	100.36	99.68	100.54	100.70	100.69
Ba	369	488	271	633	609	678	788	314	332	132
Ce	32	31	26	46	47	75	75	42	28	14
Cl	55	54	79	96	137	40	35	85	33	33
Cr	16	4	10	19	19	9	6	7	17	9
Ga	21	18	16	18	18	22	22	16	17	19
La	21	28	15	19	24	37	38	25	21	17
Nb	16	16	13	11	10	15	16	11	9	8
Nd	16	17	14	18	23	46	36	10	15	13
Ni	6	4	5	7	9	5	4	4	5	5
Pb	25	34	32	23	21	18	17	25	26	15
Rb	230	235	219	147	112	126	127	216	172	262
Sc	bdl	5	8	8	9	9	11	5	5	bdl
Sn	15	12	11	bdl	5	bdl	5	10	13	12
Sr	104	132	71	124	127	91	98	69	78	31
Th	11	13	7	12	13	12	13	14	11	6
U	9	10	7	6	6	8	5	bdl	bdl	5
V	24	13	9	33	31	19	21	11	8	7
Y	19	20	15	37	36	61	66	19	19	14
Zn	49	43	22	40	33	77	70	29	16	41
Zr	131	162	77	159	168	303	289	101	89	82

CG Central Granite, *GD* Granitic dyke, *JG* Jelen grad metagranite, *GG* Garić-grad metagranite, *VT* Vrtlinska metagranite, *GT* G. Garešnica metagranite

sequence. It often encloses biotite and plagioclase and is frequently interstitial. The plagioclase is short-prismatic, euhedral to subhedral, and it typically displays oscillatory zoning. The muscovite is a subsolidus mineral and grows, for instance, within plagioclases. Microstructures suggest that an appreciable amount of the muscovite formed by reaction from earlier cordierite. Pseudomorphs of cordierite, represented by nests of muscovite intergrown with green biotite, can frequently be seen. Since these pseudomorphs are evenly distributed, and not concentrated in schlieren or associated with assimilated country rock material, they are best interpreted as relics of early magmatic cordierite. Andalusite is a common accessory mineral (Pamić 1990). It is randomly distributed in the feldspar–quartz matrix, often euhedral, and therefore most probably of magmatic origin. In some localities tourmaline can be found.

Chemical data for the Central Granite are shown in Fig. 5 and Table 2. Generally high A/CNK ratios indicate a metasedimentary magma source. An S-type granite nature is further indicated by the generally high P and low Y contents (Chappell and White 2001). The

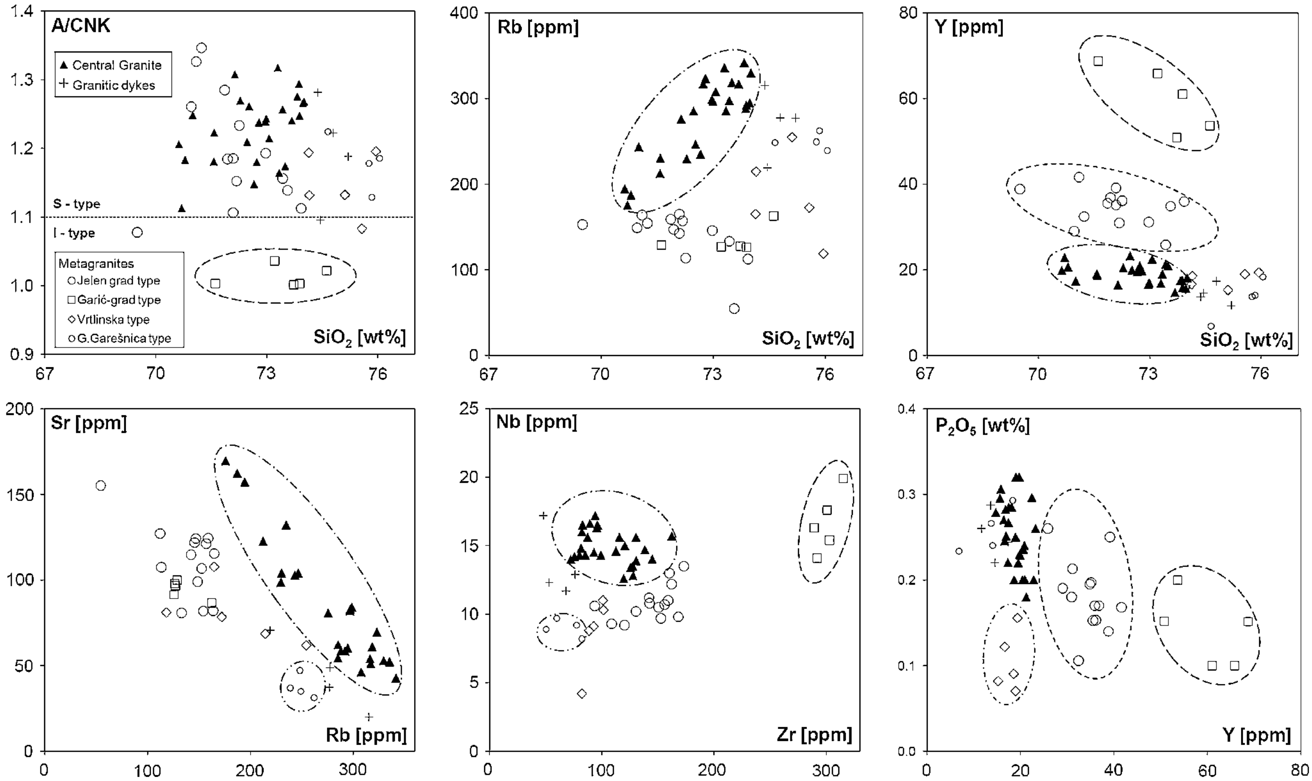

Fig. 5 Selected diagrams highlighting the most distinctive geochemical features of the various granitoid rocks of the MGM

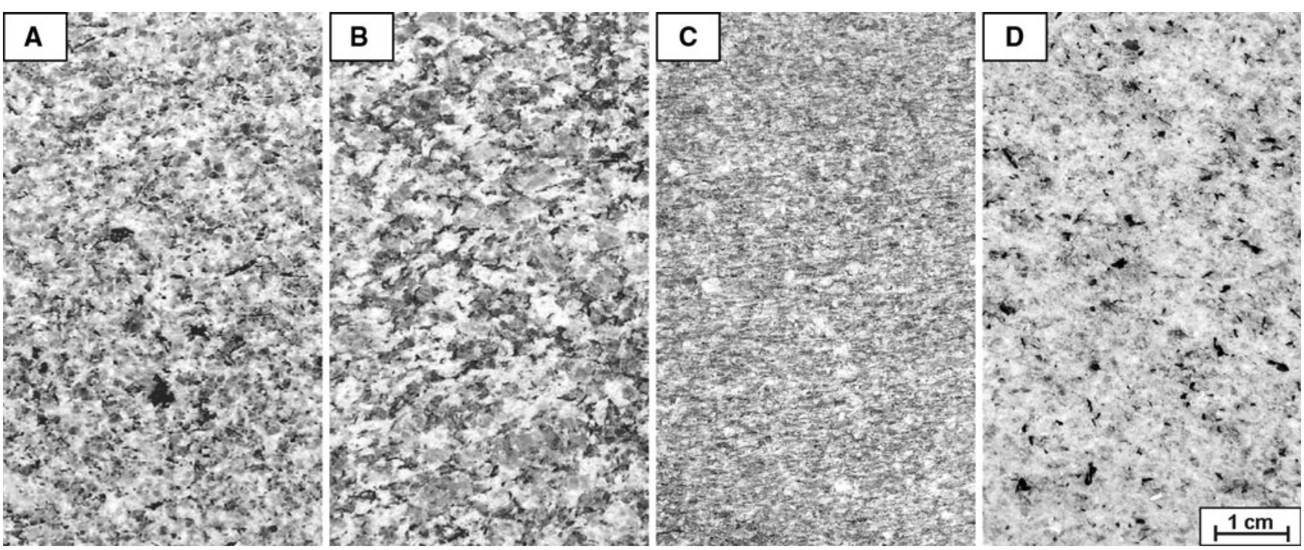

Fig. 6 Macroscopic variability of the Central Granite of the MGM. **a**, **b** Finer and coarser grained types from N of G. Jelenska. **c** Mylonitic granite from Mikleuška quarry. **d** Granite dyke from Pleterac quarry. All pictures in same magnification

thoroughly felsic nature of the Central Granite indicates that a fairly good separation of restite and melt has occurred in the source region or during an early stage of magma ascent. Chemical variations in Rb, Sr, Zr and LREE can be interpreted in terms of magmatic fractional crystallization, but show no systematic regional zoning pattern. Granitic dykes crosscutting the main granite occasionally continue into the country rocks. They deviate slightly from the main chemical evolution trend of the Central Granite Unit, for instance in the Rb–Sr ratios (Fig. 5).

The chemical diagrams in Fig. 5 illustrate that there are significant geochemical differences between the Central Granite Unit and the metagranites of the MGM.

Zircon dating

Sample preparation and analytical procedure

Five samples were selected for zircon dating, two from the Central Granite, two from the Garić-grad metagranite and one from the Jelen grad metagranite. 1–3 kg of rock material was crushed in a jaw crusher and then sieved. The fraction <400 μm was further processed on a wet shaking table in order to concentrate the heavy minerals. Magnetic minerals were removed with a permanent magnet and a Frantz Magnetic Separator. A representative selection of zircons (~200 per sample) was then handpicked and embedded in epoxy resin. Using diamond pastes, the embedded zircons were ground into their centre and polished. After carbon coating the polished zircons were imaged on a Leica Stereoscan 430 with an Oxford Mini cathodoluminescence detector. From grains that showed week CL signal, BSE photographs were additionally taken on a Jeol 8600 microprobe. The morphological parameters of the zircon populations were investigated with a transmitted-light microscope.

LA-SF-ICP-MS analyses were performed at the Institute of Geosciences, Goethe University, Frankfurt, Germany, using a Thermo-Finnigan Element II sector field ICP-MS coupled to a New Wave UP213 ultraviolet laser system. A teardrop-shaped, low volume laser cell was used to enable sequential sampling of heterogeneous grains during time resolved data acquisition (see Frei and Gerdes 2009). Zircon grains mounted in resin blocks and polished to half their thickness were analysed for ^{202}Hg, ^{204}Hg + ^{204}Pb, ^{206}Pb, ^{207}Pb, ^{208}Pb, ^{232}Th, ^{235}U and ^{238}U in peak jumping mode using a laser spot-size of 30 μm. Each analyses consisted of approximately 20 s background acquisition followed by 35 s data acquisition. The ^{204}Pb signal interferes with the ^{204}Hg isotope that occurs together with ^{202}Hg in the argon carrier gas. The precise detection of ^{204}Pb was therefore dependent on accurate monitoring of Hg. A common-Pb correction based on the calculated ^{204}Pb and a model Pb composition (Stacey and Kramers 1975) was carried out if necessary. The necessity of the correction was usually based on the ^{206}Pb/^{204}Pb (<10,000). However, in case the interference corrected ^{204}Pb could not be precisely detected (e.g. <20 cps), this was only applied when the corrected ^{207}Pb/^{206}Pb laid outwith the internal errors of the measured ratios and yielded more concordant results. Raw data were corrected for background signal, common-Pb, laser induced elemental fractionation, instrumental mass discrimination, and time-dependant elemental fractionation of Pb/Th and Pb/U using an Excel® spreadsheet program. Reported errors (2σ) were propagated with the reproducibility (2 SD) of the GJ-1 standard ($n = 12$) of the individual sequence (33 unknowns and 12 standards), which were 1.2 and 1.4% for the ^{207}Pb/^{206}Pb and ^{206}Pb/^{238}U ratios, respectively. Concordia diagrams (2 error ellipses) and concordia ages (95% confidence level) were produced using Isoplot/Ex 2.49 (Ludwig 2000). For further details on analytical protocol and data processing see Gerdes and Zeh (2009).

Zircon populations

In the Central Granite, slim, long prismatic (100–300 μm long) zircons with dominant {110} + {101} ± {211} morphology can be found (Fig. 7). Additionally, short prismatic (100–200 μm long) zircons with large pyramids {211} occur. These short prismatic crystals often consist of a large corroded core showing a bright CL signal and a thin, oscillatory zoned outer growth shell (Fig. 8). The long prismatic zircons typically display a continuous oscillatory magmatic zoning without visible cores.

The Garić-grad metagranite carries mainly stubby zircons (50–200 μm long) with large {100} and {101} crystal faces. Approximately half of the zircons exhibit a thin overgrowth zone, which is bright in the BSE image (Fig. 8). This overgrowth is interpreted as metamorphic. The zircons in the sample of Jelen grad metagranite are mostly short prismatic with large steep pyramids {211}. They show oscillatory zoning with bright inner zones in the CL images. Thin overgrowth shells are often present and interpreted as being of metamorphic origin. Classifying the zircons in terms of Pupin (1980) confirms that the Central Granite and the Jelen grad metagranite represent S-type granites, while the Garić-grad metagranite has a zircon population typical for an I- or A-type granite (Fig. 7).

Zircon ages

Garić-grad metagranite

Most measurements provided concordant U–Pb isotope data between 460 and 500 Ma (Fig. 9, Table 3). Some gave slightly younger U–Pb data which arrange along a discordia that trends towards a Cretaceous lower intersect age. The metamorphic overgrowth rims around the zircons were not targeted due to their small size. Using the oldest concordant data points, concordia ages of 486 ± 6 Ma ($n = 7$) and 483 ± 6 Ma ($n = 9$) were calculated for the two samples. These dates indicate an Early Ordovician formation age for the Garić-grad metagranite. Inheritance plays little role in the zircons, suggesting a high magma temperature (Chappell 1999; Miller et al. 2003). Only a few cores in sample BS 3 represent relictic Precambrian zircons with ages of ~600 and ~1,200 Ma, respectively (Table 3).

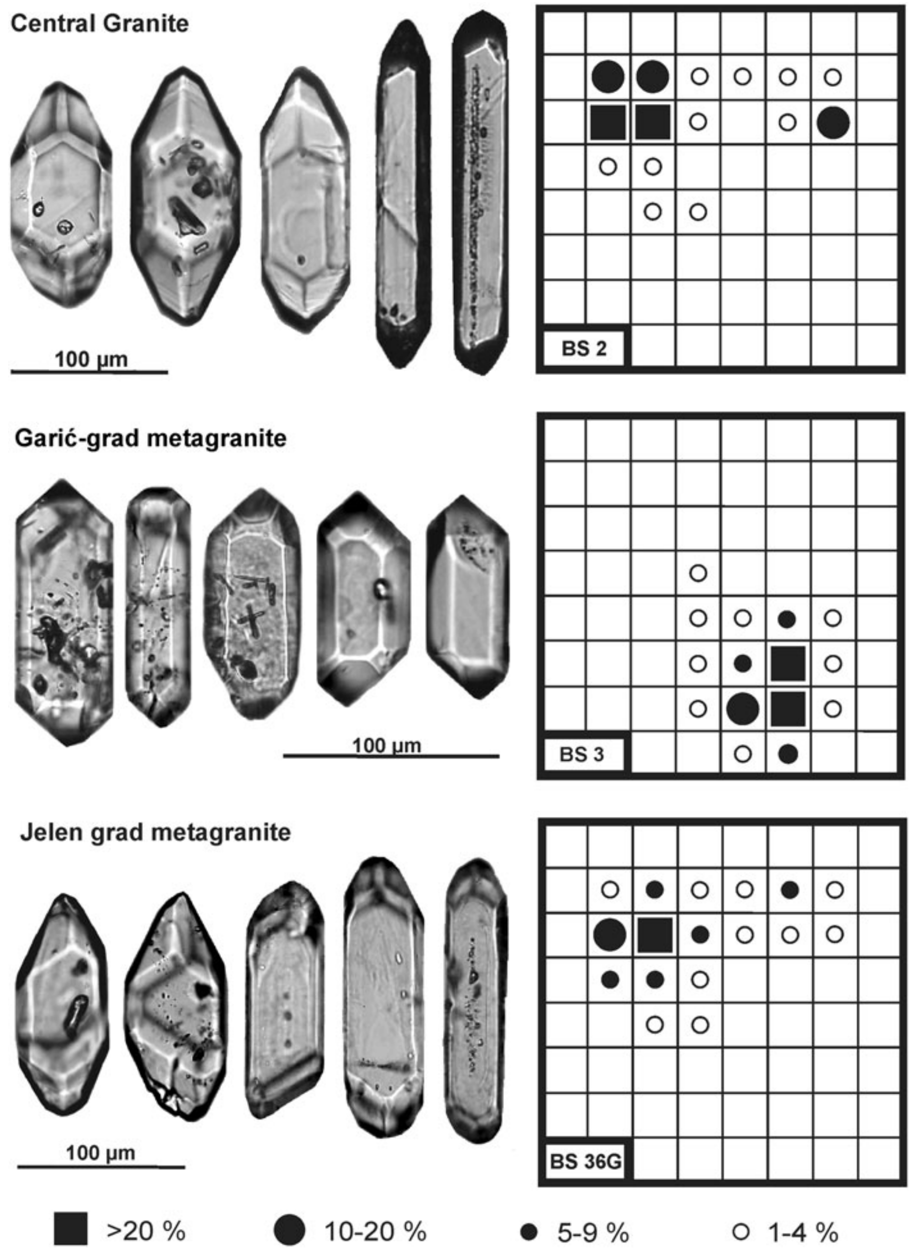

Fig. 7 Zircon morphologies in the Central Granite and the Garić-grad and Jelen grad metagranites. Diagrams according to Pupin (1980)

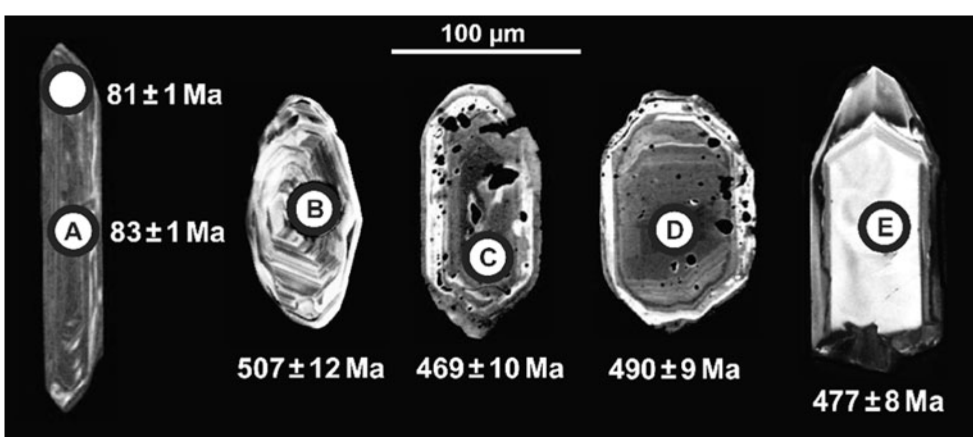

Fig. 8 Representative examples of dated zircons. **a**, **b** Zircons from the Central Granite (sample BS 2). **c**, **d** Zircons from the Garić-grad metagranite (sample BS 21a). **e** Zircon from the Jelen grad metagranite (sample BS 36G)

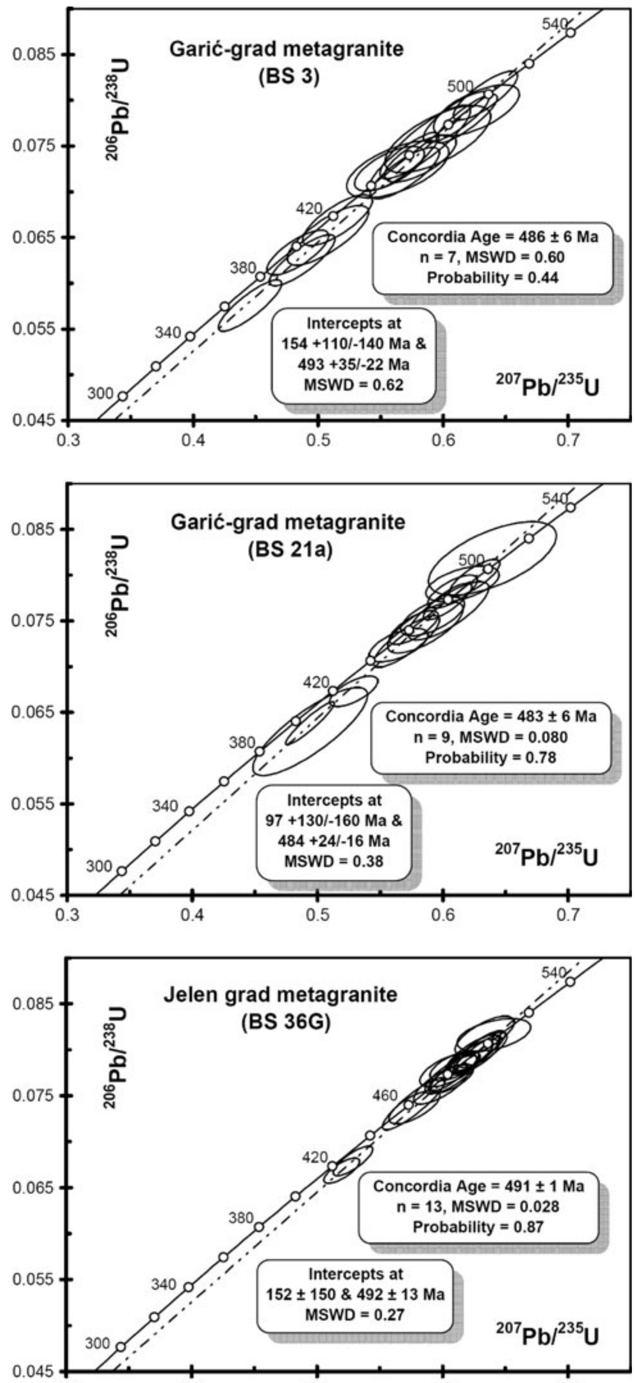

Fig. 9 Results of LA-SF-ICP-MS zircon dating for metagranites from the MGM, shown in concordia diagrams

Jelen grad metagranite

The zircons from the sample of Jelen grad metagranite provide for their most part also Early Ordovician U–Pb ages (Fig. 9, Table 3). Analyses arrange along a discordia chord, which intersects with the concordia at 152 and 492 Ma. Data ellipses that lie close to the upper intercept give a concordia age of 491 ± 1 Ma ($n = 13$). Older inherited zircon relics were rarely found. Zircon 5 (Table 3) contains an inherited core with a late Precambrian age. Zircon 11 yielded a Palaeoproterozoic age of ~3,000 Ma in its core.

Central Granite

Laser dating confirmed that many zircons of the Central Granite, in particular the larger stubby ones, have inherited cores mantled by overgrowth zones. Most of these cores gave an Early Palaeozoic age (Fig. 10, Table 3). The overgrowth zones were difficult to target with the laser. Attempts to date these rims commonly resulted in mixed ages. The group of long prismatic zircons turned out to be free of inheritance. However, these slim, needle shaped zircons were difficult to analyse as well, because they tended to break when hit by the laser beam. In sample BS 2 we were successful in analysing some of these long prismatic magmatic grains (Fig. 8). These gave concordant U–Pb data clustering around a mean concordia age of 82 ± 2 Ma (Fig. 10). In sample BS 26 the magmatic zircon growth phase could be constrained via a discordia chord defined by a number of mixing ages and one rim point at 82 ± 1 Ma (^{238}U–^{206}Pb age). Interestingly, the upper intersect age of this discordia is Permian. This implies that the Alpine rims commonly overgrow inherited Permian zircon. Many zircon grains in the Central Granite thus seem to have a threefold age zoning: an Early Palaeozoic inner core, a Permian overgrowth zone, and an outer Alpine growth shell. Laser measurements on grain 25 (Table 3) clearly document a case where an Ordovician zircon became directly overgrown by a Permian zircon.

Electron microprobe based monazite dating

Samples

Accessory monazite was encountered in samples of Central Granite (BS 1, BS 2, BS 4), Garić-grad and Jelen grad metagranite (BS 3 and BS 21a, BS 20 and BS 36G), as well as in metapelites (BS 8, BS 9, BS 10, BS 11). Monazite was searched for by means of backscattered electron imaging (BSE) on the electron microprobe and chemically dated in polished thin-sections. The monazite grains show a similar morphology in all rock types. They are mostly 10–30 μm in size and round to subhedral. Many of them exhibit a compositional zoning in the BSE image (Fig. 11).

Table 3 Results of LA-SF-ICP-MS zircon dating for the Central Granite and metagranites from the MGM

	^{207}Pb (cps)[a]	U (ppm)[b]	Pb (ppm)[b]	$\frac{^{206}P}{^{204}P}$	$\frac{Th^b}{U}$	$\frac{^{206}Pb^c}{^{238}U}$	±2σ (%)	$\frac{^{207}Pb^c}{^{235}U}$	±2σ (%)	Rho[d]	$\frac{^{207}Pb^c}{^{238}U}$	±2σ (%)	$\frac{^{207}Pb}{^{235}U}$	±2σ (Ma)	$\frac{^{206}Pb}{^{238}U}$	±2σ (Ma)	$\frac{^{207}Pb^c}{^{206}Pb}$	±2σ (Ma)	Concentration (%)[e]
Garić-grad metagranite (sample BS 3)																			
1	6,647	249	17	11,368	0.36	0.0669	3.4	0.515	2.2	0.77	0.0559	1.4	422	15	417	14	448	62	93
2	10,634	422	27	18,732	0.31	0.0633	3.1	0.484	2.1	0.76	0.0554	1.4	401	14	396	12	427	61	93
3	30,426	1,107	81	909	0.22	0.0754	4.3	0.586	2.5	0.86	0.0563	1.3	468	19	469	20	464	57	101
4	859	50	5	1,406	0.39	0.0966	5.4	0.818	4.4	0.61	0.0614	3.5	607	41	595	31	652	149	91
5	16,437	1,111	88	28,704	0.36	0.0782	2.9	0.611	1.8	0.82	0.0567	1.0	484	14	485	14	478	45	101
6	16,103	723	63	29,525	0.52	0.0805	2.7	0.634	3.3	0.82	0.0571	0.9	498	13	499	13	495	42	101
7	14,099	1,237	78	25,221	0.35	0.0625	3.7	0.487	4.4	0.83	0.0565	1.2	403	15	391	14	473	54	83
8	5,882	215	16	2,458	0.38	0.0725	3.5	0.564	5.9	0.59	0.0564	2.4	454	22	451	15	469	105	96
9	15,710	536	41	6,097	0.26	0.0780	2.8	0.619	3.2	0.86	0.0575	0.8	489	13	484	13	512	36	94
10	2,220	117	10	3,484	0.12	0.0845	3.6	0.859	7.8	0.47	0.0738	3.5	630	37	523	18	1,035	140	50
11	9,192	649	44	1348	0.37	0.0652	4.1	0.508	5.2	0.78	0.0564	1.6	417	18	407	16	470	72	87
12	7,178	327	25	5,049	0.42	0.0736	2.9	0.582	4.0	0.71	0.0573	1.4	466	15	458	13	503	62	91
13	5,278	488	29	2,955	0.39	0.0576	4.0	0.445	4.6	0.86	0.0561	1.2	374	15	361	14	457	53	79
14	21,700	1556	112	37,602	0.25	0.0733	3.5	0.569	4.0	0.87	0.0562	1.0	457	15	456	15	462	43	99
15	5,035	368	27	9,187	0.31	0.0725	2.7	0.557	4.1	0.67	0.0557	1.5	450	15	451	12	440	67	102
16	9,303	646	48	16,089	0.38	0.0720	3.2	0.569	4.0	0.80	0.0573	1.2	458	15	448	14	504	52	89
17	7,851	513	40	13,483	0.23	0.0789	2.9	0.627	4.5	0.65	0.0576	1.7	494	18	489	14	515	75	95
18	26,181	542	114	9,769	0.58	0.1936	2.7	2.115	3.1	0.87	0.0792	0.8	1,154	21	1,141	28	1,178	30	97
19	3,906	271	20	2,463	0.30	0.0758	3.9	0.596	5.8	0.68	0.0570	2.1	474	22	471	18	492	94	96
Garić-grad metagranite (sample BS 21a)																			
1	1,068	120	7	2,847	0.27	0.0629	6.3	0.494	7.6	0.82	0.0570	4.3	408	26	393	25	490	95	80
2	21,966	891	71	29,000	0.42	0.0771	2.1	0.604	2.6	0.82	0.0568	1.5	480	10	479	10	483	33	99
3	6,959	271	20	9,978	0.24	0.0743	3.1	0.586	4.2	0.73	0.0572	2.9	468	16	462	14	500	63	92
4	6,928	308	21	9,377	0.42	0.0673	2.0	0.529	3.0	0.68	0.0570	2.2	431	10	420	8	491	48	86
5	14,458	576	48	68,214	0.46	0.0797	2.1	0.625	2.6	0.79	0.0569	1.6	493	10	494	10	488	36	101
6a	12,201	263	20	7,827	0.50	0.0724	2.1	0.565	3.4	0.61	0.0566	2.7	455	12	450	9	476	60	95
6b	6,964	140	11	4,572	0.43	0.0761	3.4	0.604	4.4	0.79	0.0576	2.7	480	17	473	16	514	59	92
7	24,493	502	40	16,220	0.34	0.0782	1.9	0.608	2.7	0.71	0.0564	1.9	482	10	485	9	467	42	104
8	9,437	222	17	423,899	0.51	0.0727	3.2	0.571	3.8	0.84	0.0569	2.1	459	14	453	14	488	46	93
9	22,201	462	34	76,517	0.30	0.0743	2.0	0.577	2.8	0.73	0.0563	1.9	462	10	462	9	465	42	99
10	5,021	86	7	3,356	0.46	0.0818	4.0	0.640	6.5	0.62	0.0567	5.1	502	26	507	20	480	113	106
11	7,082	144	11	2,095	0.32	0.0755	2.3	0.592	3.5	0.65	0.0569	2.7	472	13	469	10	486	59	96
12	2,846	62	5	25,072	0.40	0.0790	2.0	0.616	3.9	0.52	0.0565	3.3	487	15	490	9	472	74	104
13	22,932	579	38	13,961	0.45	0.0638	3.0	0.494	3.2	0.93	0.0561	1.2	408	13	399	12	458	26	87

Table 3 continued

	^{207}Pb (cps)[a]	U (ppm)[b]	Pb (ppm)[b]	$\frac{^{206}P}{^{204}P}$	$\frac{Th^b}{U}$	$\frac{^{206}Pb^c}{^{238}U}$	±2σ (%)	$\frac{^{207}Pb^c}{^{235}U}$	±2σ (%)	Rho[d]	$\frac{^{207}Pb^c}{^{238}U}$	±2σ (%)	$\frac{^{207}Pb}{^{235}U}$	±2σ (Ma)	$\frac{^{206}Pb}{^{238}U}$	±2σ (Ma)	$\frac{^{207}Pb^c}{^{206}Pb}$	±2σ (Ma)	Concentration (%)[e]
Jelen grad metagranite (sample BS 36G)																			
1a	38,097	583	45	59,667	0.17	0.0793	1.9	0.625	2.6	0.74	0.0572	1.8	493	10	492	9	498	39	99
1b	36,057	567	35	121,163	0.04	0.0668	1.9	0.520	2.2	0.74	0.0564	1.5	425	8	417	8	467	33	89
2	28,262	436	34	23,557	0.22	0.0791	1.9	0.621	2.4	0.77	0.0570	1.6	491	10	491	9	491	34	100
3	15,075	246	19	14,696	0.19	0.0800	1.9	0.631	2.6	0.75	0.0573	1.7	497	10	496	9	501	37	99
4	14,087	226	16	23,827	0.07	0.0773	2.2	0.607	2.9	0.78	0.0570	1.8	482	11	480	10	491	40	98
5a	11,939	201	15	7,404	0.06	0.0778	1.9	0.605	3.1	0.63	0.0564	2.4	480	12	483	9	467	53	103
5b	20,015	203	23	10,581	0.61	0.0981	2.0	0.835	2.5	0.78	0.0617	1.6	616	12	603	11	665	34	91
6	9,119	154	11	29,859	0.21	0.0738	2.0	0.578	2.9	0.70	0.0568	2.1	463	11	459	9	483	45	95
7	14,065	178	13	3,892	0.08	0.0769	1.7	0.607	2.4	0.69	0.0572	1.8	481	9	477	8	501	39	95
8a	10,225	165	14	4,410	0.36	0.0816	1.8	0.641	3.7	0.48	0.0570	3.3	503	15	506	9	490	73	103
8b	34,124	556	37	25,918	0.12	0.0679	1.9	0.529	2.4	0.80	0.0565	1.5	431	9	424	8	471	33	90
9a	80,562	1,327	98	51,841	0.04	0.0794	2.2	0.627	2.5	0.88	0.0573	1.2	494	10	493	10	502	26	98
9b	12,223	197	15	5,483	0.23	0.0783	1.7	0.610	2.7	0.64	0.0565	2.0	484	10	486	8	473	45	103
10	17,173	268	20	57,200	0.07	0.0795	2.2	0.624	2.8	0.79	0.0569	1.7	492	11	493	11	489	38	101
11a	22,935	373	27	16,682	0.08	0.0791	2.2	0.619	3.2	0.70	0.0568	2.2	489	12	491	10	485	50	101
11b	452,868	295	206	32,796	0.70	0.5732	3.6	17.81	4.2	0.86	0.2254	2.2	2,980	42	2,921	86	3,020	35	97
12a	50,655	807	56	33,323	0.06	0.0741	3.1	0.577	3.5	0.89	0.0565	1.6	463	13	461	14	471	36	98
12b	26,995	449	33	42,796	0.05	0.0793	1.8	0.623	2.3	0.80	0.0570	1.4	492	9	492	9	492	30	100
13	24,479	359	26	6,859	0.11	0.0762	2.3	0.599	3.0	0.76	0.0570	2.0	477	12	474	10	492	44	96
14a	32,788	480	36	22,891	0.06	0.0799	2.2	0.629	2.7	0.83	0.0571	1.5	496	11	496	11	496	33	100
14b	52,993	935	67	184,651	0.04	0.0777	2.2	0.610	2.6	0.86	0.0569	1.3	483	10	482	10	489	29	99
15	19,251	229	19	24,168	0.18	0.0815	2.1	0.634	3.0	0.70	0.0564	2.2	498	12	505	10	467	48	108
Central Granite (sample BS 2)																			
1	35,949	2,512	178	3,361	0.13	0.0745	3.3	0.591	4.1	0.81	0.0576	2.4	472	16	463	15	514	53	90
2	10,704	673	57	18,780	0.41	0.0819	2.5	0.641	3.3	0.78	0.0568	2.1	503	13	507	12	484	45	105
3	8,376	622	40	14,810	0.25	0.0656	3.4	0.511	4.2	0.82	0.0565	2.4	419	14	410	14	474	52	86
4	11,068	2,301	168	1,579	0.30	0.0780	3.6	0.612	4.2	0.86	0.0569	2.1	485	16	484	17	488	47	99
5	5,996	392	34	4,455	0.46	0.0811	3.3	0.634	4.7	0.71	0.0567	3.3	499	19	503	16	481	74	104
6	5,551	354	28	9,661	0.24	0.0794	3.8	0.626	4.5	0.84	0.0571	2.4	494	18	493	18	497	54	99
7a	5,550	630	22	3,223	0.29	0.0347	6.5	0.269	7.6	0.85	0.0564	4.0	242	16	220	14	467	88	47
7b	6,034	628	65	1,080	0.07	0.1097	2.7	0.927	4.8	0.56	0.0613	3.9	666	24	671	17	650	84	103
8	4,615	703	29	8,972	0.29	0.0411	4.0	0.294	5.0	0.80	0.0519	3.0	262	12	260	10	281	68	92
9a	3,182	147	8	5,921	0.47	0.0487	2.2	0.352	3.5	0.64	0.0525	2.7	306	9	306	7	307	61	100
9b	9,692	473	25	6,071	0.49	0.0497	1.8	0.361	2.5	0.70	0.0527	1.8	313	7	313	5	315	41	99

Table 3 continued

	^{207}Pb (cps)[a]	U (ppm)[b]	Pb (ppm)[b]	$\frac{^{206}P}{^{204}P}$	$\frac{Th^{b}}{U}$	$\frac{^{206}Pb^{c}}{^{238}U}$	±2σ (%)	$\frac{^{207}Pb^{c}}{^{235}U}$	±2σ (%)	Rho[d]	$\frac{^{207}Pb^{c}}{^{238}U}$	±2σ (%)	$\frac{^{207}Pb}{^{235}U}$	±2σ (Ma)	$\frac{^{206}Pb}{^{238}U}$	±2σ (Ma)	$\frac{^{207}Pb^{c}}{^{206}Pb}$	±2σ (Ma)	Concentration (%)[e]
10	2,852	574	7	2,233	0.31	0.0126	1.9	0.083	2.7	0.69	0.0479	2.0	81	2	81	2	93	47	87
11	3,837	144	9	5086	0.43	0.0599	4.5	0.470	5.1	0.89	0.0569	2.4	391	17	375	17	488	53	77
12a	6,893	907	12	1,543	0.29	0.0126	1.7	0.083	3.8	0.46	0.0477	3.3	81	3	81	1	86	79	94
12b	7,432	1,263	17	2,342	0.29	0.0130	1.5	0.087	2.7	0.57	0.0486	2.2	85	2	83	1	128	53	65
13a	2,543	495	6	1,293	0.06	0.0128	1.4	0.085	4.0	0.36	0.0483	3.7	83	3	82	1	115	88	71
13b	4,637	726	10	994	0.29	0.0129	2.1	0.087	3.9	0.53	0.0492	3.3	85	3	83	2	155	78	53
14	4,264	785	10	2,000	0.05	0.0131	1.6	0.085	3.1	0.51	0.0473	2.7	83	3	84	1	65	63	128
15a	2,865	147	9	4,916	0.07	0.0630	2.5	0.499	4.2	0.60	0.0575	3.3	411	14	394	10	509	73	77
15b	2,560	165	10	1,289	0.09	0.0619	6.6	0.486	7.6	0.87	0.0569	3.8	402	26	387	25	487	83	79
Central Granite (sample BS 26)																			
1	77,330	3,717	55	2,794	0.68	0.0129	1.9	0.085	5.8	0.33	0.0481	5.5	83	5	82	2	105	131	79
2	11,651	183	15	40,649	0.36	0.0790	2.1	0.621	3.2	0.68	0.0570	2.3	491	12	490	10	493	52	99
3	87,688	2,943	128	2,848	0.37	0.0425	1.9	0.306	2.2	0.84	0.0523	1.2	271	5	268	5	297	32	90
4	8,348	133	11	3,929	0.25	0.0817	2.1	0.647	3.0	0.70	0.0575	2.2	507	12	506	10	509	47	99
5	12,431	221	16	3,115	0.21	0.0762	2.1	0.589	3.1	0.68	0.0561	2.3	470	12	473	10	455	50	104
6	4,172	236	6	2,365	0.33	0.0243	3.4	0.166	5.0	0.68	0.0498	3.7	156	7	154	5	184	86	84
7	11,312	402	18	8,261	0.41	0.0424	2.0	0.302	2.6	0.76	0.0517	1.7	268	6	268	5	271	39	99
8	84,361	3,650	57	2,960	0.75	0.0136	2.4	0.091	4.8	0.50	0.0488	4.1	89	4	87	2	138	97	63
9	17,155	292	22	20,949	0.18	0.0792	1.7	0.624	2.4	0.72	0.0572	1.7	492	9	491	8	498	37	99
10	8,816	145	11	6,224	0.17	0.0817	2.0	0.645	3.0	0.68	0.0573	2.2	506	12	506	10	503	48	101
11	3,284	140	11	3,349	0.16	0.0786	3.4	0.617	4.2	0.82	0.0569	2.4	488	16	488	16	488	52	100
12	28,861	2,777	62	1,033	0.53	0.0208	2.4	0.140	4.4	0.55	0.0490	3.7	133	5	133	3	146	291	91
13	9,300	155	13	5,241	0.39	0.0800	1.7	0.629	2.4	0.70	0.0570	1.8	496	10	496	8	493	39	101
14	6,684	518	23	4,908	0.37	0.0434	2.1	0.305	3.2	0.66	0.0509	2.4	270	8	274	6	238	56	115
15	12,669	1,010	46	2,256	0.41	0.0408	2.6	0.289	3.3	0.79	0.0514	2.0	258	7	258	7	259	46	100
16	1,927	46	6	695	0.79	0.1045	3.2	0.873	5.0	0.64	0.0606	3.8	637	24	641	19	625	83	103
17a	47,847	1,671	73	5,391	0.40	0.0427	2.3	0.307	2.6	0.88	0.0521	1.3	272	6	270	6	291	29	93
17b	23,271	1,793	79	4,901	0.36	0.0434	2.2	0.312	2.5	0.89	0.0523	1.1	276	6	274	6	296	31	92
17c	8,811	965	33	1,583	0.25	0.0348	2.9	0.244	3.3	0.86	0.0509	1.7	222	7	220	6	236	39	93
18	126,045	114	63	20,716	0.46	0.4902	2.3	12.46	2.5	0.92	0.1843	1.0	2,639	24	2,571	50	2,692	16	96
19	41,144	4,144	69	1,535	0.46	0.0147	6.4	0.098	6.9	0.92	0.0485	2.7	95	6	94	6	125	64	75
20a	5,818	588	21	5,390	0.39	0.0341	2.3	0.237	3.7	0.62	0.0504	2.9	216	7	216	5	212	67	102
20b	4,998	646	14	7,912	0.17	0.0233	2.1	0.162	3.9	0.54	0.0504	3.3	152	6	148	3	215	77	69
20c	7,472	447	19	14,518	0.35	0.0422	1.6	0.300	2.4	0.69	0.0516	1.7	267	6	267	4	267	39	100
21	8,086	618	27	1,560	0.38	0.0429	2.2	0.306	3.0	0.73	0.0518	2.0	271	7	271	6	276	46	98

Table 3 continued

	^{207}Pb (cps)[a]	U (ppm)[b]	Pb (ppm)[b]	$\frac{^{206}P}{^{204}P}$	$\frac{Th^b}{U}$	$\frac{^{206}Pb^c}{^{238}U}$	±2σ (%)	$\frac{^{207}Pb^c}{^{235}U}$	±2σ (%)	Rho[d]	$\frac{^{207}Pb^c}{^{238}U}$	±2σ (%)	$\frac{^{207}Pb}{^{235}U}$	±2σ (Ma)	$\frac{^{206}Pb}{^{238}U}$	±2σ (Ma)	$\frac{^{207}Pb^c}{^{206}Pb}$	±2σ (Ma)	Concentration (%)[e]
22a	6,449	116	8	5,110	0.21	0.0723	2.5	0.567	3.8	0.64	0.0568	2.9	456	14	450	11	485	65	93
22b	9,794	293	19	12,573	0.09	0.0677	1.8	0.527	2.2	0.81	0.0565	1.3	430	8	422	7	472	29	89
23	6,247	192	16	4,792	0.33	0.0819	1.8	0.643	2.6	0.69	0.0570	1.9	504	10	508	9	490	42	104
24a	2,298	58	5	3,870	0.45	0.0810	2.1	0.637	4.1	0.52	0.0570	3.5	500	16	502	10	493	77	102
24b	2,090	56	5	3,715	0.57	0.0820	2.3	0.643	3.5	0.65	0.0569	2.7	504	14	508	11	487	59	104
25a	8,885	278	22	15,322	0.35	0.0781	1.8	0.618	2.4	0.77	0.0574	1.5	488	9	485	9	506	33	96
25b	2,657	239	11	4,854	0.39	0.0443	4.0	0.317	4.7	0.87	0.0519	2.3	280	11	280	11	279	53	100
26a	3,763	97	8	2,643	0.32	0.0813	2.0	0.640	3.0	0.67	0.0571	2.2	502	12	504	10	497	49	101
26b	3,902	102	8	6,764	0.35	0.0804	1.8	0.634	2.7	0.65	0.0572	2.1	499	11	499	9	498	46	100
27	8,362	278	19	4,888	0.09	0.0742	3.3	0.583	3.7	0.89	0.0570	1.7	466	14	461	15	492	36	94

Sample locations: BS 3, BS 21a: road cuts near Garić-grad ruin; BS 36G: Jelen grad ruin; BS 2: Pleterac quarry; BS 26: 3.5 km W of Šimljanik

[a] Within run background-corrected mean ^{207}Pb signal

[b] U and Pb content and Th/U ratio were calculated relative to GJ-1 reference zircon

[c] Corrected for background and within-run Pb/U fractionation (in case of $^{206}Pb/^{238}U$) and common Pb using Stacey and Kramers (1975) model Pb composition and subsequently normalised to GJ-1 (ID-TIMS value/measured value); $^{207}Pb/^{235}U$ calculated using $^{207}Pb/^{206}Pb/(^{238}U/^{206}Pb*1/137.88)$

[d] Rho is the error correlation defined as $err^{206}Pb/^{238}U/err^{207}Pb/^{235}U$

[e] Degree of concordance = $^{238}U/^{206}Pb/^{207}Pb/^{206}Pb$ *100

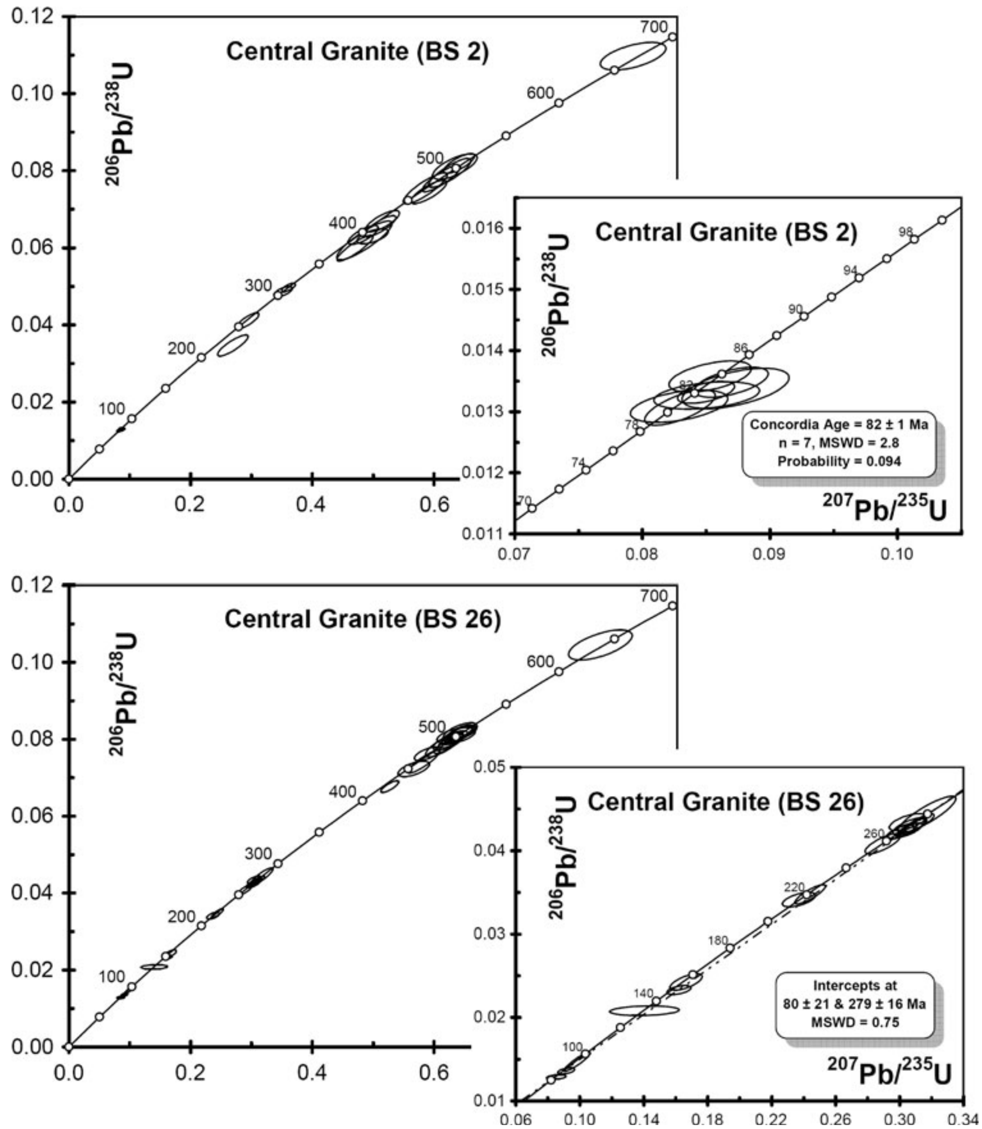

Fig. 10 Results of LA-SF-ICP-MS zircon dating for the Central Granite from the MGM, shown in concordia diagrams

Analytical procedure

Monazite analyses followed the routine established at the Mineralogical Department of Salzburg University (Finger and Broska 1999; Krenn et al. 2008). This involves a complete WD monazite analyses for elements Si, P, As, S, La, Ce, Pr, Nd, Sm, Gd, Dy, Y, Th, U, Ca and Pb. Prolonged counting times for Th, U and Pb enable a calculation of moderately precise Th–U–Pb ages, following the method of Montel et al. (1996). The analytical errors of a point analyses typically correspond to a $\sim$20–60 Ma error on the age (2σ). A weighted average age with reduced error can be calculated from a larger number of measurements in coherent age domains. Results were controlled using standard monazite F5 with a concordant ID-TIMS age of 341 Ma. A detailed and up to date description of standards, element lines, counting times, background positions, interference corrections, etc., currently used in Salzburg is given in Krenn et al. (2008).

Obtained ages

Central Granite

Measurements in Th- and U-rich magmatic monazite from sample BS 1 (leucocratic dyke of Central Granite from Srednja rijeka) can be combined to a weighted average age of 80 $\pm$ 5 Ma. This age is consistent with the magmatic zircon age of 82 $\pm$ 1 Ma obtained for the Central Granite by LA-SF-ICP-MS dating. Monazite average ages obtained from samples BS 2 and BS 4 are less precise (84 $\pm$ 22, 96 $\pm$ 29 Ma), which is mainly due to lower radiogenic Pb contents, but corroborate a Cretaceous formation age for the whole Central Granite Unit. A systematic age

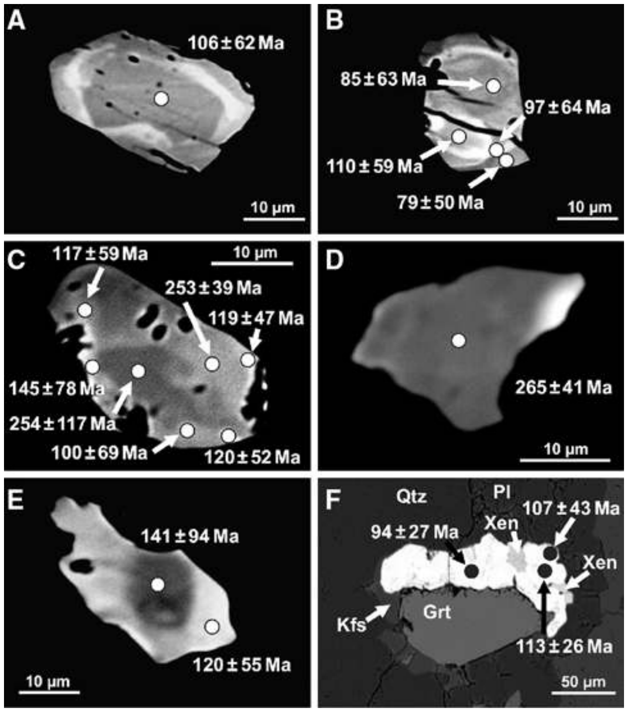

Fig. 11 BSE images of dated monazites. **a**, **b** Metapelite, sample BS 10. **c**, **d** Metapelite, sample BS 9. **e** Central Granite, sample BS 4. **f** Garić-grad metagranite, sample BS 21a

difference between monazite core and rim zones could not be resolved.

Garić-grad and Jelen grad metagranites

Monazite in the metagranites formed in the Cretaceous. Average ages for samples BS 20, BS 36G (Jelen grad type) and BS 21a (Garić-grad type) are 92 ± 11, 90 ± 35, and 95 ± 16 Ma and considered as dating the LP/HT metamorphic stage. In sample BS 3 (Garić-grad type), a xenotime grain has been additionally measured. It shows also a Cretaceous total Pb age (103 ± 22 Ma). In the Garić-grad metagranite, xenotime typically forms in paragenesis with monazite (Fig. 11f), probably owing to the Y rich geochemistry of the bulk rock (see Fig. 5).

The maximum Y content of the monazite (~3.5 wt% Y_2O_3) can be used to estimate metamorphic temperatures, based on the monazite–xenotime miscibility thermometer of Heinrich et al. (1997). From this geothermometer monazite formation temperatures of ~750°C can be inferred. This result is consistent with the P–T data derived from the metapelitic lithologies (see "The metapelites") and corroborates the concept that the MGM underwent a granulite facies LP/HT regional metamorphism during the Cretaceous. An inherited monazite core with an apparent age of 211 ± 23 Ma (most probably a mixing age) has been found in sample BS 21a.

Metapelite samples

Three of the four investigated samples carry Cretaceous monazite populations, for which mean ages of 95 ± 21, 95 ± 16, and 99 ± 14 Ma have been calculated. Although the ages are relatively imprecise, they cluster between 90 and 100 Ma like the monazite ages obtained for the metagranites. This implies that the LP/HT metamorphism in the MGM probably took place between 90 and 100 Ma. Distinct core zones are often visible in the BSE images (e.g. Fig. 11a, b) which seem to be resorbed and overgrown by new monazite. However, an age difference between these core and rim zones could mostly not be measured. This may be due to the only moderate precision of electron microprobe dating. A multiple growth of monazite by dissolution reprecipitation is a common feature in high grade monazite. It may occur, within a short time span of a few million years, during the same metamorphic cycle (Finger and Krenn 2007). Only in one mica schist sample we found clear evidence for an older monazite population with a Permian age of 276 ± 18 Ma (Table 4). The Permian monazite grains in this sample show only narrow Alpine overgrowth zones (Fig. 11).

Discussion and conclusions

Geochronological constrains

The geochronological investigations carried out in the frame of this work demonstrate the following:

1. The Central Granite Unit of the MGM represents a Late Cretaceous intrusion. The pooled U–Pb concordia age of 82 ± 1 Ma obtained from magmatic zircon is in accordance with Ar–Ar muscovite cooling ages of 73 ± 1 and 74 ± 1 Ma for pegmatite dykes derived from the Central Granite (Palinkaš et al. 2000; Balen et al. 2001).
2. The metamorphic country rocks, into which the Central Granite intruded, were subjected to granulite facies LP/HT metamorphism in the Mid Cretaceous, most probably between 90 and 100 Ma. This age estimate, which is based on EMP monazite dating, is consistent with amphibole (cooling) ages of 80–90 Ma reported for amphibolitic rocks from the metamorphic complex (Lanphere and Pamić 1992; Balen et al. 2001). Although the timing of this LP/HT event remains to be more precisely constrained in future work, it is clear from the monazite ages that the high-grade metamorphic history of the MGM is Alpine and not Variscan.

Table 4 U–Th–Pb ages of monazites from Central Granite, metagranites and metapelites from the MGM

	Th (wt%)	U (wt%)	Pb (wt%)	Th* (wt%)	Age ± 2σ (Ma)
Central Granite (sample BS 1)					
m 2.1	3.870	0.984	0.016	7.004	53 ± 30
m 2.2	4.606	2.601	0.050	12.911	87 ± 16
m 4	3.682	1.070	0.022	7.096	71 ± 29
m 6.1	9.250	6.342	0.103	29.494	79 ± 7
m 6.2	8.326	4.616	0.084	23.064	82 ± 9
m 6.3	5.869	2.576	0.053	14.095	85 ± 15
					80 ± 5
Central Granite (sample BS 2)					
m 3	6.083	0.836	0.028	8.749	71 ± 24
m 4	5.641	0.496	0.034	7.226	106 ± 29
m 7	5.928	0.383	0.030	7.151	94 ± 29
m 8.1	4.473	0.095	0.015	4.775	71 ± 44
m 8.2	3.804	0.035	0.019	3.915	109 ± 53
m 8.3	3.700	0.376	0.010	4.898	48 ± 43
					84 ± 22
Central Granite (sample BS 4)					
m 1	5.993	0.198	0.028	6.625	94 ± 31
m 2.1	5.410	0.140	0.023	5.857	88 ± 61
m 2.2	3.074	0.125	0.010	3.473	65 ± 104
m 4.1	5.460	0.116	0.008	5.828	29 ± 62
m 4.2	5.128	0.101	0.025	5.450	103 ± 66
m 5.1	3.467	0.108	0.024	3.811	141 ± 94
m 5.2	6.009	0.169	0.035	6.548	120 ± 55
m 6.1	3.743	0.105	0.032	4.079	178 ± 88
					96 ± 29
Garić-grad metagranite (sample BS 3)					
m 1.1	1.761	0.430	0.012	3.133	84 ± 115
m 1.2	1.971	0.410	0.011	3.280	78 ± 110
m 1.3	1.770	0.417	0.010	3.101	71 ± 117
					78 ± 64
x 1.1	0.946	1.474	0.025	5.659	101 ± 64
x 1.3	1.654	2.657	0.041	10.144	91 ± 36
x 1.4	0.513	0.955	0.013	3.562	83 ± 102
x 1.5	0.808	1.057	0.027	4.200	147 ± 86
x 1.6	1.631	2.494	0.047	9.611	111 ± 38
					103 ± 22
Garić-grad metagranite (sample BS 21a)					
m 1.1	4.242	0.670	0.062	6.404	216 ± 28
m 1.2	3.579	0.693	0.051	5.809	199 ± 44
					211 ± 23
m 2	4.645	1.775	0.047	10.319	102 ± 18
m 4.1	5.919	0.270	0.028	6.782	94 ± 27
m 4.2	3.522	0.744	0.028	5.903	107 ± 43
m 4.3	7.079	0.808	0.049	9.665	113 ± 26
m 5	5.595	1.920	0.042	11.722	81 ± 15
					95 ± 16

Table 4 continued

	Th (wt%)	U (wt%)	Pb (wt%)	Th* (wt%)	Age ± 2σ (Ma)
Jelen grad metagranite (sample BS 20)					
m 1	4.572	0.836	0.031	7.243	96 ± 29
m 3	4.251	3.501	0.071	15.447	103 ± 14
m 5.1	4.014	0.187	0.019	4.609	91 ± 78
m 5.2	3.706	1.467	0.025	8.385	67 ± 43
m 6.1	3.518	4.072	0.073	16.536	99 ± 13
m 6.2	3.685	3.500	0.052	14.858	80 ± 17
m 6.3	3.840	3.571	0.055	15.241	82 ± 14
					92 ± 11
Jelen grad metagranite (sample BS 36G)					
m 1	4.080	0.266	0.018	4.928	80 ± 37
m 2	4.050	0.662	0.019	6.160	71 ± 29
m 5	4.264	1.040	0.037	7.592	110 ± 24
m 7	1.999	0.186	0.007	2.592	64 ± 70
					90 ± 35
Metapelite (sample BS 8)					
m 2	4.503	0.605	0.023	6.435	82 ± 56
m 4	4.621	0.404	0.010	5.906	40 ± 61
m 5	4.780	0.554	0.034	6.552	116 ± 32
m 6	0.911	0.660	0.007	3.013	50 ± 120
m 7	3.892	0.762	0.027	6.328	95 ± 57
					95 ± 21
Metapelite (sample BS 9)					
m 2	3.308	0.328	0.052	4.369	265 ± 41
m 3	4.032	0.353	0.070	5.176	302 ± 40
m 4	2.443	0.142	0.037	2.904	283 ± 71
m 5	3.694	0.523	0.069	5.389	286 ± 38
m 6.1	4.148	0.380	0.061	5.374	253 ± 39
m 6.2	1.201	0.178	0.020	1.776	254 ± 117
					276 ± 18
m 6.3	6.122	0.251	0.037	6.925	120 ± 52
m 6.4	4.159	0.409	0.029	5.468	119 ± 47
m 6.5	3.907	0.678	0.031	6.076	117 ± 59
m 6.6	3.733	0.278	0.030	4.623	145 ± 78
m 6.8	4.174	0.322	0.023	5.203	100 ± 69
					119 ± 25
Metapelite (sample BS 10)					
m 1	3.947	0.314	0.023	4.949	103 ± 36
m 2.1	4.242	0.466	0.022	5.730	85 ± 63
m 2.2	4.648	0.299	0.024	5.604	97 ± 64
m 2.3	4.869	0.731	0.025	7.202	79 ± 50
m 2.4	4.817	0.420	0.030	6.161	110 ± 59
m 3.1	4.814	0.368	0.021	5.988	81 ± 60
m 4.1	4.256	0.439	0.026	5.659	104 ± 64
m 4.2	4.045	0.485	0.021	5.592	84 ± 65
m 4.3	4.134	0.520	0.027	5.797	106 ± 62
m 4.4	2.943	0.640	0.025	4.989	113 ± 72
m 5	4.972	0.277	0.028	5.858	106 ± 62

Table 4 continued

	Th (wt%)	U (wt%)	Pb (wt%)	Th* (wt%)	Age ± 2σ (Ma)
m 6.1	4.201	0.488	0.015	5.756	59 ± 63
m 6.2	4.958	0.192	0.025	5.573	100 ± 65
					95 ± 16
Metapelite (sample BS 11)					
m 1.1	4.920	0.723	0.031	7.230	96 ± 29
m 1.2	2.491	0.403	0.017	3.779	102 ± 96
m 1.3	4.292	0.446	0.016	5.714	65 ± 63
m 1.4	4.785	0.568	0.016	6.594	56 ± 55
m 1.5	2.469	0.514	0.022	4.113	120 ± 88
m 2	7.704	0.648	0.047	9.775	109 ± 21
m 3	1.889	0.404	0.015	3.180	103 ± 114
m 4	5.293	0.691	0.028	7.499	84 ± 48
m 5	1.251	0.214	0.010	1.935	114 ± 187
m 6	3.255	0.589	0.029	5.141	125 ± 70
					99 ± 14

Errors are 2σ for single analyses. Weighted average ages in bold were calculated at the 95% confidence level

3. The main rock types within the metamorphic mantle of the MGM, the orthogneisses and diatexites, are derived from Early Ordovician granitic protholiths.
4. There is some evidence that the MGM was affected by magmatic and metamorphic events during the Permian. Indications for Variscan tectonothermal events are as yet missing.

The pre-Alpine evolution of the MGM

All three dated samples of metagranites provided the same Early Ordovician formation age. We therefore conclude that the metamorphic complex of the MGM represents for a great part remnant Ordovician granitic crust. Geochemical data allow distinguishing of four different subunits of metagranites. The volumetrically dominant Jelen grad type metagranites define a coarse grained, K-feldspar phyric, S-type granite suite. Ordovician granitic rocks of this kind are widespread in the Alpine basement and also in the Bohemian Massif (e.g. von Raumer et al. 2002). They are commonly interpreted in terms of crustal melting in an extensional setting (rifting of the northern Gondwana margin). A-type granites, as represented by the Garić-grad metagranites of the MGM, can be taken as indications for a rift setting as well (Pitcher 1983). Due to its generally felsic nature it is likely that the Ordovician granite plutonism in the MGM resulted mainly from high-T lower crustal melting. However, the chemical signature of the Ordovician granite magmatism is clearly different from that of the Cretaceous granitic magmatism in the MGM (Central Granite Unit), although the latter is also derived from lower crustal melting. From the lower degree of zircon inheritance it may be concluded that the Ordovician magmas were much hotter.

The protolith ages of the amphibolites in the MGM are yet unknown. These rocks are often intercalated in the Ordovician granitoid rocks. Therefore, it may be that they represent Ordovician intrusions as well. It is a well known fact that the Early Palaeozoic magmatism in Central Europe fairly often has a bimodal character (Pin 1990), and this may hold true also for the MGM.

The sedimentation age of the metapelites of the MGM is unknown. We presume that this is pre-Ordovician, but since it cannot be fully ruled out that the metapelites and the orthogneisses are in a tectonic and not intrusive contact, a post-Ordovician (e.g. Mid Palaeozoic or Carboniferous) age is also possible.

A very remarkable point is that there is as yet no safe evidence for Variscan imprints in the MGM. This lack of a Variscan record constitutes a clear difference between the MGM and the Papuk, Psunj and Krndija massifs of the Slavonian Mountains, where Variscan granites and Variscan metamorphic rocks are widespread (Pamić and Lanphere 1991; Pamić et al. 1996). This observation may support the recent tectonic concepts of Ustaszewski et al. (2008) and Schmid et al. (2008), according to which the MGM is not a part of the Tisia terrane, as previously interpreted (Pamić 1998; Pamić and Jurković 2002). Of course, it can be argued that the traces of an eventually present Variscan metamorphic event in the MGM were obliterated by the strong Cretaceous LP/HT regional metamorphism. The MP metamorphism recorded in amphibolitic rocks of the MGM (Pamić et al. 2002a) could be theoretically a Variscan feature, but this is by no means certain. The fact that Variscan zircons play no role in the inherited zircon spectrum of the Central Granite is an additional argument to suggest that the MGM was not strongly affected by Variscan magmatism and metamorphism.

Given the lack of a Variscan record, it is the more interesting that geochronological evidence for Permian metamorphic and magmatic events was encountered in the MGM. The inherited Permian zircons in the Central Granite are suggestive of Permian magmatism or anatexis in the lower crust. The Permian monazites found in one sample of metapelite most probably document a Permian phase of metamorphism in the metamorphic series of the MGM. It would thus appear that the MGM was part of a zone within the Pangea continent that experienced Permian crustal extension in the forefield of the Alpine orogenic cycle (Schuster et al. 2001).

The Alpine evolution of the MGM

The emplacement of the Central Granite at ~80 Ma belongs to the latest endogenic processes documented in the present day outcrop level of the MGM. Post-granitic, greenschist facies deformation is found in the SE part of the MGM. The mica ages in this area are 70–80 Ma (Lanphere and Pamić 1992; Palinkaš et al. 2000; Balen et al. 2001), suggesting that deformation occurred not long after the Central Granite intruded. These late greenschist facies deformation processes in the MGM may be related to the late Cretaceous orogenic activity recorded in other parts of the Sava Zone (e.g. the Motajica Massif, Krenn et al. 2008), and interpreted as collisional tectonics between the Northern Dinarides and the Tisia block (Schmid et al. 2008; Ustaszewski et al. 2008).

Retrogression and alteration under lower amphibolite facies conditions is an ubiquitous feature in the metamorphic series of the MGM and is also seen in rocks that show no strong late shearing. We believe that the penetrative retrograde metamorphism in the metamorphic mantle of the MGM was mainly caused by heat and fluid input from the Central Granite. The presence of magmatic andalusite in the Central Granite indicates an intrusion depth of <8 km (Spear et al. 1999). The previous LP/HT regional metamorphism, which imprinted the MGM in the Mid Cretaceous, occurred at pressures of 3–4 kbar, which means that the metamorphic complex was at a depth of ~10–13 km at that time. Between this stage (at 90–100 Ma) and the emplacement of the Central Granite (82 Ma), a considerable uplift of the MGM could have occurred. One can thus speculate that the granite formation was triggered by decompression melting processes in the lower crust of the MGM. The relatively fast cooling of the Central Granite indicated by mica ages (Lanphere and Pamić 1992; Palinkaš et al. 2000; Balen et al. 2001) implies that its intrusion took place at a time when the metamorphic rocks of the MGM were already cold. We therefore believe that the Central Granite Unit cannot be directly related with the Cretaceous high-T metamorphic stage, and formed some million years later, probably during a stage of crustal uplift.

Most enigmatic is the LP/HT characteristics of the Mid Cretaceous metamorphism in the MGM, which is a very unusual feature in the Alpine belt. Possibly, this LP/HT metamorphism represents only a relatively small structure, which reflects a locally increased heat flow induced for instance through a hot mafic intrusion. During our field work in the MGM, we found no evidence for mafic magmatism of Alpine age. However, Balen et al. (2003) reported a find of a boulder of an olivine gabbro in the Kamenjača valley (south of Humka, Fig. 1) that they dated at 109 ± 8 Ma. In addition, a diabase body with a hornblende age of 110 ± 7 Ma (Pamić et al. 2002b) was discovered in a borehole from the South Pannonian Basin (Sava Depression). This may support the idea that the Mid Cretaceous LP/HT metamorphism in the MGM is related to a local magmatic underplating of mafic mantle magma. While the Tisia block was magmatically quiet at that time (Schmid et al. 2008; Ustaszewski et al. 2008), gabbroic supra-subduction zone intrusions of Senonian age have been recently reported from the Dinarides (Božović et al. 2008).

Acknowledgments The paper greatly benefited from the constructive comments of Bruce Chappell, Vladica Cvetković, Alfons Berger, and another anonymous journal reviewer, and by the thorough editorial handling of Edwin Gnos. Andreas Mayer is gratefully acknowledged for his support during field work and sample preparation. Erwin Krenn and Bernhard Humer kindly helped with the electron microprobe work. Biljana Starijaš wants to thank the staff members and colleagues from the Mineralogical and Geological Departments for various supports during her PhD stay at Salzburg University. This work received funding through project 18070 of the Austrian Science Foundation (to F. Finger). Travel costs were partly covered by bilateral (Austria-Croatia) scientific cooperation programs (to D. Balen and F. Finger).

References

Balen, D. & Pamić, J. 2000. Crystalline Complex of Mt. Moslavačka Gora. In: J. Pamić & B. Tomljenović (Eds) *PANCARDI 2000 fieldtrip guidebook* (pp. 44–47). Dubrovnik.

Balen, D., Schuster, R., & Garašić, V. (2001). A new contribution to the geochronology of Mt. Moslavačka Gora (Croatia). PANCARDI 2001 Abstracts II, Sopron, DP-2.

Balen, D., Schuster, R., Garašić V., & Majer, V. (2003). The Kamenjača olivine gabbro from Moslavačka Gora (South Tisia, Croatia). Rad Hrvatske akademije znanosti i umjetnosti 486, Knjiga XXVII, 57–76.

Barić, Lj. (1954). Biotitno-kordijeritni škriljavac s andaluzitom i silimanitom iz Jaske potoka u Moslavačkoj gori. *Geologija, 2*, 145–157.

Božović, M., Prelević, D., Gerdes, A., Romer, R.L., Barth M., Cvetković V., & van den Bogaard, P. (2008). Oceanic crust production in the Dinarides during the Senonian: Combined U–Pb in situ laser ablation ICP(MC)-MS zircon and mineral separates Ar–Ar dating. *EGU General Assembly 2008: Geophysical Research Abstracts 10*, Vienna.

Chappell, B. J. (1999). Aluminium saturation in I- and S-type granites and the characterization of fractionated haplogranites. *Lithos, 46*, 535–551.

Chappell, B. J., & White, A. J. R. (1974). Two contrasting granite types. *Pacific Geology, 8*, 173–174.

Chappell, B. J., & White, A. J. R. (2001). Two contrasting granite types: 25 years later. *Australian Journal of Earth Sciences, 48*, 489–499.

Collins, W. J., Beams, S. D., White, A. J. R., & Chappell, B. W. (1982). Nature and origin of A-type granites with particular reference to southeastern Australia. *Contributions to Mineralogy and Petrology, 80*, 189–200.

Csontos, L., & Nagymarosy, A. (1998). The Mid-Hungarian line: A zone of repeated tectonic inversions. *Tectonophysics, 297*, 51–71.

Finger, F., & Broska, I. (1999). The Gemeric S-type granites in southeastern Slovakia: Late Palaeozoic or Alpine intrusions? Evidence from electron-microprobe dating of monazite. *Schweizerische Mineralogische und Petrographische Mitteilungen, 79*, 429–443.

Finger, F., & Krenn, E. (2007). Three metamorphic monazite generations in a high-pressure rock from the Bohemian Massif and the potentially important role of apatite in stimulating polyphase monazite growth along a PT loop. *Lithos, 95*, 103–115.

Frei, D., & Gerdes, A. (2009). Accurate and precise in situ zircon U–Pb age dating with high spatial resolution and high sample throughput by automated LA-SF-ICP-MS. *Chemical Geology, 261*, 261–270.

Gerdes, A., & Zeh, A. (2009). Zircon formation versus zircon alteration—new insights from combined U–Pb and Lu–Hf in situ La-ICP-MS analyses of Archean zircons from the Limpopo Belt. *Chemical Geology, 261*, 230–243.

Gessmann, C. K., Spiering, B., & Raith, M. (1997). Experimental study of Fe–Mg exchange between garnet and biotite: Constraints on the mixing behavior and analysis of the cation-exchange mechanisms. *American Mineralogist, 82*, 1225–1240.

Green, N. L., & Usdansky, S. I. (1986). Toward a practical plagioclase-muscovite thermometer. *American Mineralogist, 71*, 1109–1117.

Heinrich, W., Andrehs, G., & Franz, G. (1997). Monazite-xenotime miscibility gap thermometry I. An empirical calibration. *Journal of Metamorphic Geology, 15*, 3–16.

Hoisch, T. D. (1989). A muscovite-biotite geothermometer. *American Mineralogist, 74*, 565–572.

Holdaway, M. J. (2000). Application of new experimental and garnet Margules data to the garnet-biotite geothermometer. *American Mineralogist, 85*, 881–892.

Holdaway, M. J., & Lee, S. M. (1977). Fe–Mg cordierite stability in high-grade pelitic rocks based on experimental, theoretical and natural observations. *Contributions to Mineralogy and Petrology, 63*, 175–198.

Holdaway, M. J., Mukhopadhyay, B., Dyar, M. D., Guidotti, C. V., & Dutrow, B. L. (1997). Garnet-biotite geothermometry revised: New Margules parameters and a natural specimen data set from Maine. *American Mineralogist, 82*, 582–595.

Kleeman, U., & Reinhardt, J. (1994). Garnet-biotite thermometry revised: The effect of Al^{IV} and Ti in biotite. *European Journal of Mineralogy, 6*, 925–941.

Korolija, B., Vragović, M., Crnko, J., & Mamužić, P. (1986). Osnovna geološka karta 1:100 000. Tumač za list Bjelovar L 33–82. Geološki zavod Zagreb (1985), Savezni geološki zavod, Beograd.

Koziol, A. M. (1989). Recalibration of the garnet-plagioclase-Al_2SiO_5-quartz (GASP) geobarometer and application to natural parageneses. *EOS (Transactions of the American Geophysical Union), 70*, 493.

Krenn, E., Ustaszewski, K., & Finger, F. (2008). Detrital and newly formed metamorphic monazite in amphibolite-facies metapelites from the Motajica Massif, Bosnia. *Chemical Geology, 254*, 164–174.

Kretz, R. (1983). Symbols for rock-forming minerals. *American Mineralogist, 68*, 277–279.

Lanphere, M., & Pamić, J. (1992). K-Ar and Rb-Sr ages of Alpine granite-metamorphic complexes in the northwestern Dinarides and the southwestern part of the Pannonian Basin in northern Croatia. *Acta Geologica, 22*, 97–111.

Ludwig, K. R. (2000). *User's manual for Isoplot/Ex version 2.2: A geochronological toolkit for Microsoft Excel*. Berkeley Geochronology Center Special publication 1a.

Mehnert, K. R. (1968). *Migmatites and the origin of granitic rocks* (p. 393). Amsterdam: Elsevier.

Miller, C. F., McDowell, S. M., & Mapes, R. W. (2003). Hot and cold granites? Implications of zircon saturation temperatures and preservation of inheritance. *Geology, 31*, 529–532.

Montel, J. M., Foret, S., Veschambre, M., Nicollet, Ch., & Provost, A. (1996). Electron microprobe dating of monazite. *Chemical Geology, 131*, 37–53.

O'Brien, P. J. (2000). The fundamental Variscan problem: High-temperature metamorphism at different depths and high-pressure metamorphism at different temperatures. In: W. Franke, V. Haak, O. Onken, & D. Tanner (Eds), *Orogenic processes: Quantification and modelling in the Variscan Belt* (Vol. 179, pp. 369–386). London: Geological Society, Special publications.

Palinkaš, L. A., Balogh, K., Strmić, S., Pamić, J., & Bermanec, V. (2000). Ar/Ar dating and fluid inclusions study of muscovite from the pegmatite Srednja Rijeka, within granitoids of Moslavačka Gora Mt., North Croatia. In: B. Tomljenović, D. Balen, & B. Saftić (Eds.) *PANCARDI 2000 Special Issues Abstracts* (pp. 95–96). Vijesti 37/3.

Pamić, J. (1990). Alpine granites, migmatites and metamorphic rocks from Mt Moslavačka Gora and the surrounding basement of the Pannonian Basin (Northern Croatia, Yugoslavia). *Rad Jugoslovenske Akademije Znanosti i Umjetnosti, 10*, 7–121.

Pamić, J. (1998). Crystalline basement of the South Pannonian Basin based on surface and subsurface data. *Nafta, 49*, 371–390.

Pamić, J., Balen, D., & Tibljaš, D. (2002a). Petrology and geochemistry of orthoamphibolites from the Variscan metamorphic sequences of the South Tisia in Croatia—an overview with geodynamic implications. *International Journal of Earth Sciences (Geologische Rundschau), 91*, 787–798.

Pamić, J., Gušić, I., & Jelaska, V. (2000). Basic geological features of the Dinarides and South Tisia. In: J. Pamić & B. Tomljenović (Eds), P*ANCARDI 2000 Fieldtrip Guidebook* (pp. 9–18). Vijesti 37/2.

Pamić, J., & Jurković, I. (2002). Paleozoic tectonostratigraphic units of the northwest and central Dinarides and the adjoining South Tisia. *International Journal of Earth Sciences (Geologische Rundschau), 91*, 787–798.

Pamić, J., & Lanphere, M. (1991). Hercynian granites and metamorphic rocks from the Mts Papuk, Psunj, Krndija and the surrounding basement of the Pannonian Basin in Slavonija (northern Croatia). *Geologija, 34*, 81–253.

Pamić, J., Lanphere, M., Park, M., & Belak, M. (1996). Hercynian I-type and S-type granitoids from the Slavonian mountains (southern Pannonian Basin, northern Croatia). *Neues Jahrbuch für Mineralogie (Abhandlungen), 171*, 155–186.

Pamić, J., Tomljenović, B., & Balen, D. (2002b). Geodynamic and petrogenetic evolution of Alpine ophiolites from the central and NW Dinarides: An overview. *Lithos, 65*, 113–142.

Perchuk, L. L. (1991). Mineral thermodynamics and equilibria for geothermobarometry: An introduction. In: L. L. Perchuk (Eds), *Progress in metamorphic and magmatic petrology* (Vol. 503). London: Cambridge University Press.

Pin, C. (1990). Variscan oceans: Ages, origins and geodynamic implications inferred from geochemical and radiometric data. *Tectonophysics, 177*, 215–227.

Pitcher, W. S. (1983). Granite types and tectonic environment. In K. Hsu (Ed.), *Mountain building processes* (pp. 19–40). London: Academic Press.

Pupin, J. P. (1980). Zircon and granite petrology. *Contributions to Mineralogy and Petrology, 73*, 207–220.

Schmid, S. M., Bernoulli, D., Fügenschuh, B., Matenco, L., Schefer, S., Schuster, R., et al. (2008). The Alpine–Carpathian–Dinaridic orogenic system: Correlation and evolution of tectonic units. *Swiss Journal of Geosciences, 101*, 139–183.

Schmid, S. M., Fügenschuh, B., Kissling, E., & Schuster, R. (2004). Tectonic map and overall architecture of the Alpine orogen. *Eclogae geologicae Helvetiae, 97*, 93–117.

Schuster, R., Scharbert, S., Abart, R., & Frank, W. (2001). Permo-Triassic extension and related HT/LP metamorphism in the Austroalpine— Southalpine realm. *Mitteilungen der Gesellschaft der Geologie & Bergbaustudenten Österreichs, 45*, 111–141.

Spear, F. S., Kohn, M. J., & Cheney, J. T. (1999). P–T paths from anatectic pelites. *Contributions to Mineralogy and Petrology, 134*, 17–32.

Stacey, J. S., & Kramers, J. D. (1975). Approximation of terrestrial lead isotope evolution by a two-stage model. *Earth and Planetary Science Letters, 26*, 207–221.

Thompson, A. B. (1976). Mineral reactions in pelitic rocks: I Prediction of P-T-X(Fe-Mg) phase relations. II. Calculations of some P-T-X(Fe-Mg) phase relations. *American Journal of Science, 276*, 401–454.

Ustaszewski, K., Schmid, S. M., Fügenschuh, B., Tischler, M., Kissling, E., & Spakman, W. (2008). A map-view restoration of the Alpine–Carpathian–Dinaridic system for the Early Miocene. *Swiss Journal of Geosciences, 101*(Supplement 1), 273–294.

von Raumer, J. F., Stampfli, G. M., Borel, G., & Bussy, F. (2002). Organization of pre-Variscan basement areas at the north-Gondwana margin. *International Journal of Earth Sciences, 91*, 35–52.

Zwart, H. J., & Dornsiepen, U. F. (1978). The tectonic framework of Central and Western Europe. *Geologie en Mijnbouw, 57*, 627–654.